MULTIFUNCTIONAL METAL-DIELECTRIC PHOTONIC STRUCTURES

by

KYLE J. SMITH, B.S.

DISSERTATION
Presented to the Graduate Faculty of
The University of Texas at San Antonio
in Partial Fulfillment
of the Requirements
for the Degree of

DOCTOR OF PHILOSOPHY IN PHYSICS

COMMITTEE MEMBERS:
Andrey Chabanov, Ph.D., Chair
Xomalin Peralta, Ph.D.
Chonglin Chen, Ph.D.
Rafael Lopez-Mobilia, Ph.D.
Wilhelmus Geerts, Ph.D.

THE UNIVERSITY OF TEXAS AT SAN ANTONIO
College of Sciences
Department of Physics & Astronomy
Fall 2016

DEDICATION

This work is dedicated to my friends and family, for their love, support, and constant motivation. I'd like to also dedicate my work to Mr. Terry Hankins for the showing me that physics is easy, exciting, and my calling. And above all, to Bonnie; I simply could not have done this without you.

ACKNOWLEDGEMENTS

MULTIFUNCTIONAL METAL-DIELECTRIC PHOTONIC STRUCTURES

Kyle J. Smith, PhD.
The University of Texas at San Antonio, 2016

Supervising Professor: Andrey A. Chabanov, PhD.

In RF circuits and integrated photonics, it is important to effectively control an electromagnetic signal. This includes protecting of the network from high power and/or undesired signal flow, which is achieved with device functionalities such as isolation, circulation, switching, and limiting. In an attempt to develop light-weight, small-footprint, better protection devices, new designs have been sought utilizing materials that have been otherwise avoided due to some primary downside. For example, ferromagnetic metals like Iron and Cobalt, despite being powerful magnets, have been completely shunned for uses in nonreciprocal devices due to their overwhelming electric losses and high reflectivity. How could we utilize lossy materials in electromagnetic applications?

In this thesis research, we design and fabricate metal-dielectric photonic structures in which metal can be highly transmissive, while the desired response (e.g., magneto-photonic response) is strongly enhanced. Moreover, the metal-dielectric structures can be designed to exhibit a sharp transition from the induced transmission to broadband opacity for oblique incidence and/or due to a tiny alteration of the photonic structure (e.g., because of nonlinearity). Thus, the photonic structures can be tailored to produce collimation and power-limiting effects. In the case of ferromagnetic metals, the metal-dielectric structure can be realized as an omnidirectional isolator passing radiation in a single direction and for a single frequency. The effectiveness of such structures will be verified in microwave measurements. Additionally,

metal-dielectric structures including a nonlinear component will be shown to function as a reflective power limiter, thus providing a far superior alternative to absorptive, and often sacrificial, limiters.

Table of Contents

LIST OF TABLES

LIST OF FIGURES

MOTIVATION

In RF circuits and optical communication systems, new photonic devices are developed to efficiently manipulate the amplitude, phase, direction, and polarization of electromagnetic signals. Within a network, each device has a particular function, which fundamentally stems from the light-matter interactions of respective components of the given device. One such function is the protection of other devices, which can be done by the rejection or re-direction of radiation; among such devices are limiters and isolators.

Limiters are non-linear devices which can limit the power of radiation; a typical limiter uses a non-linear absorption component which passes low power signal and absorbs the excess energy when past a certain threshold. Due to overheating, however, such devices are sacrificial and thus are not sustainable. Because of this, there is need for a protection scheme which can survive the limiting process.

Isolators are nonreciprocal devices which allow the propagation of light only in one direction; they are especially used in the protection of sources from unwanted reflection. The cornerstone in the isolator design is the nonreciprocal component, e.g. a magnetic material, which rotates the plane of polarization along the axis of an applied static magnetic field; this in conjunction with polarizers allows transmission to take place in only one direction. Indeed, for standard microwave and optical isolators, magnetic ceramic materials known as ferrites are common as nonreciprocal components due to their large rotating power. However, when considering the necessary miniaturization techniques for on-chip photonic circuits, ferrite-based isolator designs become limited. In particular, because of the reduction in size, ferrites are not capable of provided quality rotation without being too bulky or needing too large of a magnetic bias. Additionally, any enhancement designs are not capable of increasing the rotation without

1

some accompanied increase in attenuation. Therefore, there is a demand for a suitable replacement to ferrites in the miniaturization viewpoint that also decouples attenuation loss from large rotation.

Recently, magneto-photonic structures have been shown to have selective enhancement where the desired light-matter interactions are enhanced while unwanted losses are reduced for a broad frequency range [1]. Namely, the reduction of losses is related to the fact that in most cases the absorption and useful functionality of a particular magnetic material are related to different components of the permittivity and/or permeability tensors ϵ and μ; and with this, the physical and geometrical characteristics for the photonic structure can be adjusted so that the electromagnetic field distribution inside the photonic structure suppresses losses and enhances the useful functionality. Such a design can be used to innovate the limiter and isolator applications. Additionally, such photonic structures can enable uses of lossy magnetic materials, such as ferromagnetic metals, which otherwise have superior magnetic properties but are avoided due to the high conductivity losses.

In this work, we design and fabricate photonic structures based on the absorption suppression mechanism described above. We will discuss how these designs can be used as a power limiter and isolator. In the case of limiters, a more sustainable limiter design will be developed to reflect, instead of absorb, electromagnetic radiation. In the case of isolators, a magneto-photonic structure will be designed and fabricated that will suppress unwanted losses in ferromagnetic metals while enhancing the magneto-optic interactions to provide Faraday rotation which is large enough to be used in conventional isolators. This will be done despite the high conductivity losses well-known to ferromagnetic metals. The same structure may also have strong directionality: transmitting radiation in a given direction and for a given frequency. These

two properties combined can lead to novel photonic functionality, namely omni-directional isolation.

The organization of this document is the following: Chapter one will first provide an essential background of periodic photonic structures to establish a foundation for our photonic structure design. This introduction will be followed with a description of the computational methods used to simulate any layered photonic structures. In chapter two, we will showcase the absorption suppression mechanism in a photonic structure that induces transmission through a metallic layer. This same photonic structure will be expanded upon in chapter three and four as a reflective power limiter and microwave isolator, respectively. The last chapter will discuss the experimental success of such designs.

CHAPTER 1: BACKGROUND & METHODS

1.1: Photonic Crystals

1.1.1: A History

Photonic crystals are periodic structures often comprised of dielectric materials of differing refractive index. The term was first used after the seminal works of Yablonovitch and John in 1987 [2, 3] but much work began nearly one hundred year earlier. In 1887, Lord Rayleigh first studied one-dimensional photonic crystals in the form of periodic multilayer dielectric stacks [4]. These dielectric stacks (later referred to as Bragg mirrors), as Rayleigh found, would provide total reflection at a frequency which characteristically was related to the periodicity of the periodic multilayer. Furthermore, this reflection existed for a range of frequencies depending on the refractive indices. This spectral range of high reflectivity would be called the photonic bandgap as transmission through such structures was forbidden for these frequencies; these structures, and its field of study, would be referred to as optical filters. For the next century, the work of Rayleigh would be expanded into the field of optical filters [5] that would lead to the development of anti-reflection and high reflectance coatings, Fabry-Perot interferometers [6], and induced transmission filters [7].

It was this bedrock that led Yablonovitch and John to the development of two and three-dimensional versions of such devices. These types of structures would be deemed photonic crystals and the same moniker would later envelop the field of optical filters.

1.1.2: The Bragg Mirror

The most common type of one-dimensional photonic crystal (PC) would be the Bragg mirror, also sometimes called the Bragg Reflector or Distributed Bragg Reflector (DBR). This type of 1-D PC is simply a periodic stack of dielectric layers which alternate between high and low refractive indices. Bragg mirrors, given their name, are known for their high reflectance. In their ideal form, each layer is "tuned" to a characteristic or reference wavelength λ_0. Specifically, to construct one such Bragg mirror, the optical thickness, nd, the product of the refractive index n and the layer thickness, d, of each layer must be equal to one quarter of a desired reference wavelength, $nd = \lambda_0/4$. This particular tuning would guarantee that multiple reflections inside the layered structure would constructively interfere for wavelengths equal to the reference wavelength. Depending on the number of dielectric layers and their refractive indices, this reflection can be well-defined and maintained for a spectral region known as the photonic band gap or stop band.

The photonic band gap and its associated reflectance are shaped by the number of layers and their respective refractive indices. Consider the following convention of layers to be either high (*H*) refractive index or low (*L*) refractive index. A common 1-D dielectric stack can be notated as

$$HLHL \dots H = (HL)^N H \qquad (1.1)$$

$$H \quad L \quad H \quad L \qquad\qquad H$$
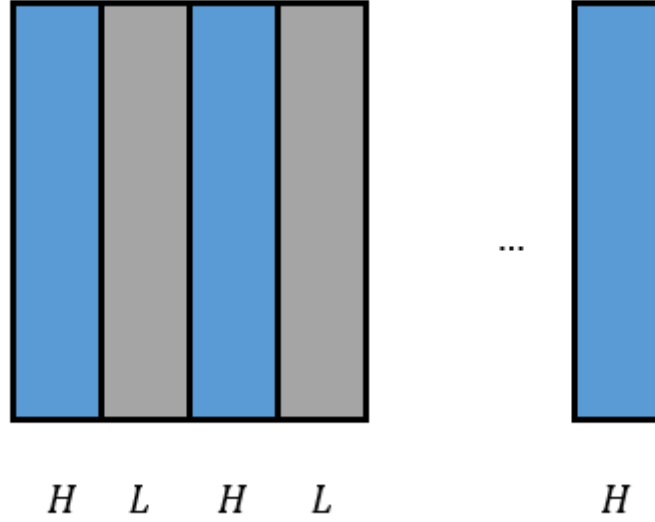
Figure 1.1 Diagrammatic Symmetric Bragg Mirror

where a unit cell comprised of one high and one low refractive index material "HL" is repeated N times. If we place another high (H) index material at the end, the structure will become symmetric for any value N. For such a structure, the reflectance can be determined using Transfer Matrix Methods (See section 1.2) where each layer is represented a matrix and manipulated as such. The reflectance at the given reference wavelength λ_0 is defined as

$$R = 1 - 4\left(\frac{n_L}{n_H}\right)^{2N} \frac{n_s}{n_H^2} \qquad\qquad (1.2)$$

Here, the $n_H, n_L,$ and n_s are the refractive indices of the high, low, and substrate materials (in the structure provided in Equation 1.1 and Figure 1.1, I assume no substrate; just free space). We see that the value of the reflectance is dependent on the index contrast $\left(\frac{n_L}{n_H}\right)$ of the dielectric materials used as well as the number of unit cells (N) in the stack. Reflection not only takes place

at the reference wavelength but throughout the band gap. This suggests that the condition of constructive interference for reflection happens for wavelengths other than λ_0, see Figure 1.2
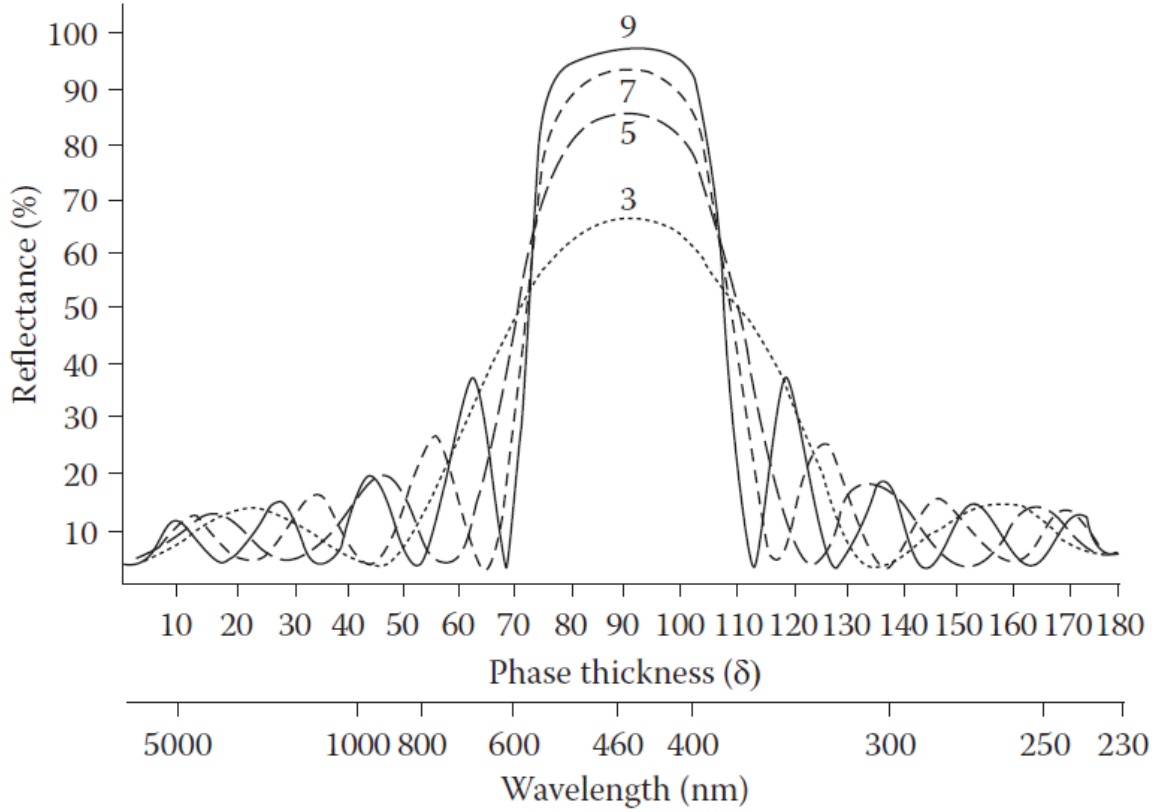
Figure 1.2 Reflectance R for normal incidence of alternating $\lambda_0/4$ layers of high ($n_H = 2.3$) and low-index ($n_L = 1.38$) dielectric materials on a transparent substrate ($n_s = 1.52$) as a function of the phase thickness $\delta = 2\pi nd/\lambda_0$ (upper scale) or the wavelength λ for $\lambda_0 = 460$ nm (lower scale). The number of unit cells are shown as a parameter on the curves [5, 6]

The nature of wave propagation in periodic media is analogous to the motion of electrons in crystals. In other words, there is a mathematical equivalence between Kronig and Penney's description of electrons in a periodic potential [8] and electromagnetic waves in periodic layered media. By extension of this analogy, we can state that any mode corresponding to the photonic band gap will be an evanescent mode (modes with imaginary eigenvalues); modes outside this

7

band gap are propagating modes (modes with real eigenvalues). It is this transition from propagation to evanescent modes (or real to imaginary eigenvalues) which can be used to determine the size of the photonic band gap [5]

$$\Delta g = \frac{2}{\pi} \sin^{-1}\left(\frac{n_H - n_L}{n_H + n_L}\right) \tag{1.3}$$

where $g = \lambda/\lambda_0$. Equation 1.3 gives the half width of the photonic band gap. We see that unlike the reflectance, the size of the photonic band gap only depends on the refractive index contrast but not the number of unit cells. This suggests that the photonic band gap exists for any number of unit cells; despite this, we can see the band gap becomes more well-defined with increasing N (See Fig. 1.1). Figure 1.3 showcases the change in photonic band gap as a function of refractive index contrast.
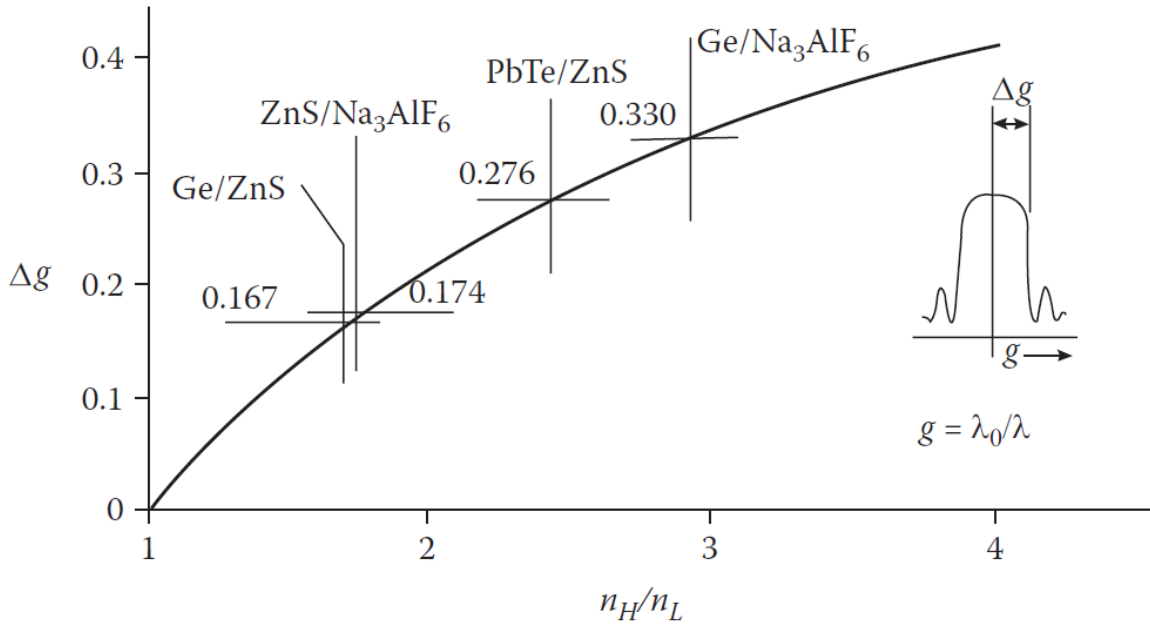
Figure 1.3 The width of the high reflectance zone (photonic band gap) of a quarter wave dielectric stack plotted against the ratio of the refractive indices, n_H/n_L [5]

Although Bragg mirrors exhibit high reflectance, the finite size of the photonic band gap implies regions of transmission; these regions are called the transmission bands or pass bands. In the transmission band, transmission resonances occur when multiple reflection destructively interfere; such transmission resonances are called Fabry-Perot resonances. The interaction of photons in structures like the Bragg mirror again cater to the analogy of electrons in periodic media, and thus structures like the Bragg mirror are sometimes referred to as one-dimensional photonic crystals. It is by the extension of this analogy that one can arrive at regions such as a photonic bandgap or transmission band.

1.1.3: Fabry-Perot Filter

Fabry-Perot filters refer to a class of narrow band pass filters which exhibit high transmission in a small frequency band bounded by regions of reflection. The Fabry-Perot [9, 10] namesake has been prescribed to a number of devices, such as the interferometers (or etalon); the essential design consists of two reflecting components separated by a spacer. Such a design insures that multiple reflections will occur inside the spacer. The conditions for constructive interference of the transmitted or reflected wave are dependent on the optical thickness of the spacer layer, as well as the angle of incidence. The simplest design will yield a transmission spectrum of successive high transmission resonances, called Fabry-Perot resonances (See Fig 1.4)
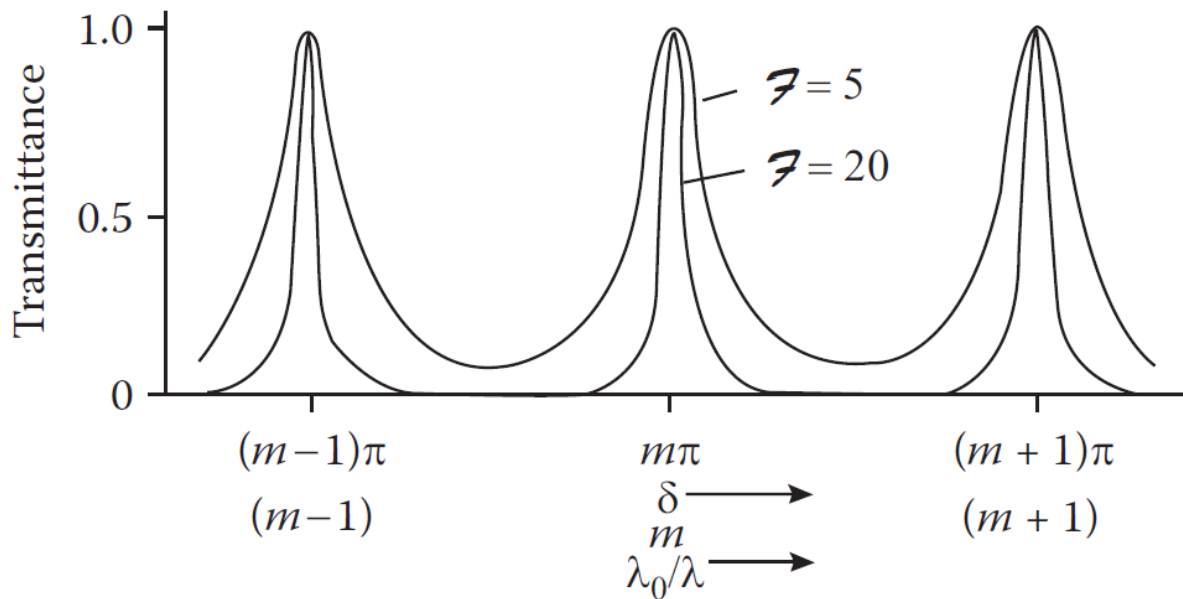
Figure 1.4 Fabry-Perot Resonances [5]

These resonances are the result of constructive interference of the transmitted wave. Their location in wavelength (or frequency) is based on the condition that makes the phase thickness δ of the spacer layer an integer multiple of π (in other words, $\delta = m\pi$). The size and separation of each resonance can also be shaped by the reflectivity of the filter, namely the reflective components. Formally, the characteristics of these resonances are described by the *Finesse* ($\mathcal{F}$) of the resonance which is defined as the ratio of the separation of adjacent resonances to the half-width [5]. The finesse can also be stated as a function of the reflectivity.

Another way to describe the attributes of these resonances is by the quality factor (or Q factor), which is the measure of the full-width half-max (FWHM) normalized by the frequency of the resonance. High performance narrow band pass filters will exhibit high Q resonances.

The development of high performance Fabry-Perot filters lies in the determination of quality reflecting components. By increasing the reflection that takes place at the boundaries of the spacer layer, one can achieve much higher Q resonances (higher finesse). For example, for a single slab of dielectric material, reflection can be increased by creating higher refractive index contrast between the dielectric material and its surroundings. The reflection can further be increased with the addition of metal layers on either side of this dielectric, however this additional reflection is often ubiquitous and thus can hinder transmission. Although the metal-dielectric-metal type Fabry Perot filter can be optimized to provide suitable transmission and reflection (such as in induced transmission filters [11]), the ultimately absorption and otherwise unwanted reflection of metals has led to the development of an all-dielectric alternative.

Figure 1.5 All-Dielectric Fabry-Perot Filter with Quarter Wavelength Structure [5]

An all-dielectric Fabry-Perot filter with high reflecting Bragg mirrors has been used as a common solution to this problem [12]. In Figure 1.5, we show one type of such a device which consists of two identical Bragg mirrors in succession, each with quarter-wavelength layers. The combination of two high index layers at the center creates a half-wave layer which acts as the spacer layer. The spacer layer will serve as a cavity and provide a resonance at the reference wavelength (note that a half wavelength layer as a spacer layer will have a phase thickness equal to π, thus matching the first condition of generating a Fabry-Perot resonance), while simultaneously constructing a photonic band gap centered at this wavelength (See Figure 1.6).
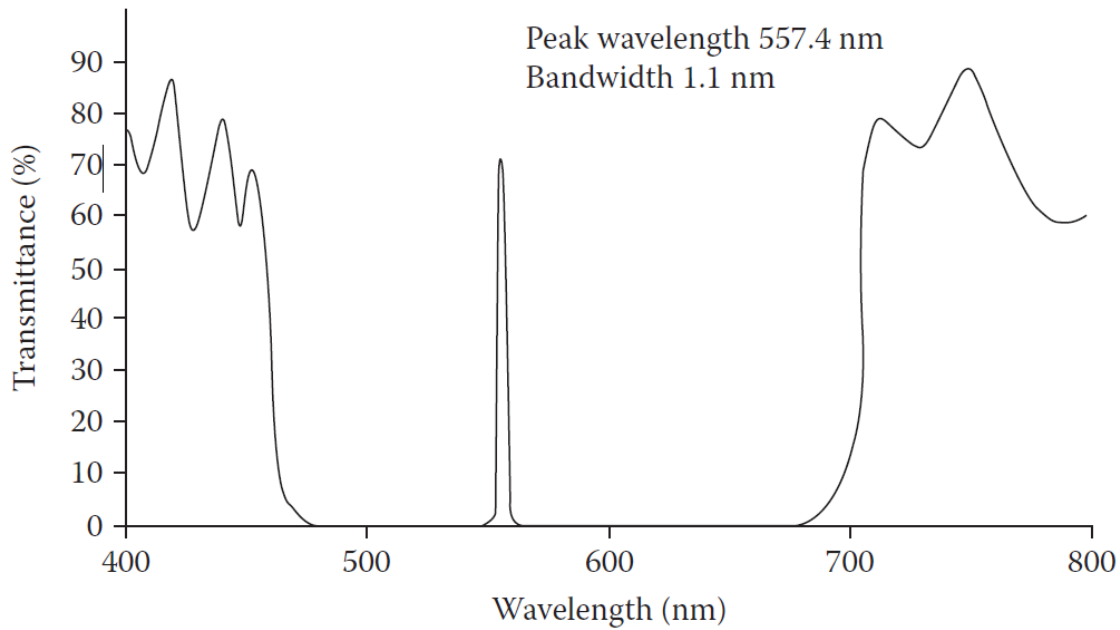
Figure 1.6 Characteristic Transmission Spectrum for a Typical All-Dielectric Fabry-Perot Filter [5].

Another point of view of the same structure is a larger single Bragg mirror with a central defect to the periodicity. The presence of the defect inside this structure creates a localized propagating mode and thus transmission can occur, the frequency location of this mode is dependent on the size and refractive indices of the layers as well as the defect; the transmission spectrum of such a structure is shown in Figure 1.6. It is based on this secondary description that this All-Dielectric Fabry-Perot Filter is sometimes referred to as a *one-dimensional defect photonic crystal* as it is the defect that creates the transmission resonance. The corresponding transmission resonance inside the photonic bandgap is sometimes then referred to as the defect mode resonance although it is still a Fabry Perot resonance.

This All-Dielectric Fabry-Perot Filter, deemed also as a one-dimensional defect photonic crystal, can serve as a quality narrow band pass filter because it provides a high Q resonance in a region of complete rejection. When such a structure is tuned as a quarter wavelength structure (with half wave spacer defect), the defect mode resonance will occur at the center of the photonic band gap. The Q factor as well as the rejection of the photonic band gap can both be tailored with refractive index contrast and number of unit cells in each Bragg mirror.

1.2: Transfer Matrix Methods

1.2.1: Introduction

The transfer matrix (TM) method is a finite element method used to analyze the propagation of electromagnetic radiation in stratified (layered) media. This method considers that each medium can be represented as a matrix and thus the combination of media can be represented as the multiplication of matrices. This method arises from the boundary conditions at the interfaces between each medium, namely the fact that both electric and magnetic fields must be continuous. The TM method works for many different geometries, but our primary use will be with one-dimensional media where only the finite size of the medium along one direction, the normal propagation direction (z direction), becomes important. The three-dimensional stack of layers can be represented and simulated as a one-dimensional stack when the size of the layers along the non-normal propagation directions (x and y directions) are much larger than that in the z direction, allowing us to ignore diffraction effects, leakage, etc. This method is well-versed and has been described in a variety of texts [7, 13, 14].

1.2.2: The Transfer Matrix

The transfer matrix $T(z_1, z_0)$ is an operator that maps the electromagnetic wave vector $\Psi(z_0)$ at location z_0 to the wave vector $\Psi(z_1)$ at location z_1.

$$\Psi(z_1) = \widehat{T}(z_1, z_0)\Psi(z_0), \qquad \Psi(z) = \begin{bmatrix} E_x(z) \\ E_y(z) \\ H_x(z) \\ H_y(z) \end{bmatrix} \tag{1.4}$$

Here we have defined the wave vector $\Psi(z)$ as a function of only the tangential components of the electric and magnetic fields. This definition, in conjunction with the continuity of tangential components across a boundary, insures that a layered stack can be represented as a collection of transfer matrices. Specifically, the transfer matrix of a layered stack $\widehat{T}_S$ is equivalent to the ordered product of each transfer matrix, $\widehat{T}_m$, inside the stack

$$\widehat{T}_S = \prod_m \widehat{T}_m \tag{1.5}$$

Where m is an integer representing the order of the stack.

The strict definition of the "transfer matrix" can vary depending on the definition of Ψ (for example, a 2 x 2 description can be found in ref. [7, 13]). We however will take a 4 x 4 transfer matrix approach. In all cases, each individual transfer matrix $\widehat{T}_m$ will be a function of the given layer's thickness d_m, permittivity ϵ_m, and permeability μ_m, and wavelength λ.

If we consider the form of Ψ in equation 1.4, the following must be true.

$$\partial_z \Psi(z) = i\frac{\omega}{c} M(z)\Psi(z) \tag{1.6}$$

Equation 1.6 can be derived from Maxwell's equations (See Appendix A) and contains a new

operator M known here as the reduced Maxwell operator [15, 16]. M is a 4 x 4 matrix which is

related to the parameters of the media, namely the permittivity and permeability. Substituting

Equation 1.4 into 1.6, we can see that the transfer matrix must satisfy the same equation.

$$\partial_z \widehat{T}(z_m, \epsilon_m, \mu_m) = i \frac{\omega}{c} M(\epsilon_m, \mu_m) \widehat{T}(z_m, \epsilon_m, \mu_m) \tag{1.7}$$

Solving the differential equation, we find

$$\widehat{T}(z_m, \epsilon_m, \mu_m) = \exp\left[i \frac{\omega}{c} z_m M(\epsilon_m, \mu_m, \vec{n})\right] \tag{1.8}$$

Where equation 1.8 is the exponential of the matrix M. Using the definition of M found in

Appendix A, an analytic solution for the transfer matrix is easily found when the media of

consideration is more simple such as isotropic or gyrotropic media [16-18]; otherwise numerical

techniques must be considered

1.2.3: Reflection and Transmission

When an electromagnetic wave Ψ^I travels through a lossless medium and arrives at a boundary, some of the wave can become reflected Ψ^R off the boundary, or transmit Ψ^T through the boundary (in the lossy case, some absorption will take place). The same can be said about a stack of layers. To determine the reflection and transmission of a stack of layers, we can use the transfer matrix associated with the stack to map the forward and backward (reflected) wave to the forward (transmitted) wave at the back of the stack. Recalling Equation 1.4 and Faraday's Law, one can state:

$$\Psi^T = \widehat{T}\Psi_0 = \widehat{T}(\Psi_0^I + \Psi_0^R),$$

$$\Psi_0^I = \begin{bmatrix} E_x \\ E_y \\ -aE_x - bE_y \\ cE_x + aE_y \end{bmatrix}, \qquad \Psi_0^R = \begin{bmatrix} \rho_x \\ \rho_y \\ a\rho_x + b\rho_y \\ -c\rho_x - a\rho_y \end{bmatrix}, \qquad \Psi^T = \begin{bmatrix} \tau_x \\ \tau_y \\ -a\tau_x - b\tau_y \\ c\tau_x + a\tau_y \end{bmatrix} \qquad (1.9)$$

Here, the subscripted zero refers to the front of the stack. The use of Faraday's law allows one to write the wave vector Ψ strictly in terms of electric field only. The reflected and transmitted electric field components are defined by (ρ_x, ρ_y) and (τ_x, τ_y), respectively; these components are referred to as reflection and transmission coefficients and are in general complex amplitudes so phase information can be extracted from them. The coefficients (a, b, c) appear after the application of Faraday's law and are defined below.

$$a = \frac{n_x n_y}{n_z}, \qquad b = \frac{(1 - n_x^2)}{n_z}, \qquad c = \frac{(1 - n_y^2)}{n_z} \qquad (1.10)$$

The coefficients (a, b, c) are in terms of a normalized wave vector $\vec{n} = \frac{c}{\omega}\vec{k} = (n_x, n_y, n_z)$ and

they are responsible for the consideration of oblique incidence. It is clear that by Equation 1.9

and the definitions in Equation 1.10, one can solve for $(\tau_x, \tau_y, \rho_x, \rho_y)$ [See Appendix B].

$$
\begin{bmatrix} \tau_x \\ \tau_y \\ \rho_x \\ \rho_y \end{bmatrix} = \hat{\Gamma}^{-1}\hat{T} \begin{bmatrix} E_x \\ E_y \\ -aE_x - bE_y \\ cE_x + aE_y \end{bmatrix} \tag{1.11}
$$

Where

$$
\hat{\Gamma} = \begin{bmatrix} 1 & 0 & -(T_{11} + aT_{13} - cT_{14}) & -(T_{12} + bT_{13} - aT_{14}) \\ 0 & 1 & -(T_{21} + aT_{23} - cT_{24}) & -(T_{22} + bT_{23} - aT_{24}) \\ -a & -b & -(T_{31} + aT_{33} - cT_{34}) & -(T_{32} + bT_{33} - aT_{34}) \\ c & a & -(T_{41} + aT_{43} - cT_{44}) & -(T_{42} + bT_{43} - aT_{44}) \end{bmatrix} \tag{1.12}
$$

The determination of the transmission and reflection coefficients, $(\tau_x, \tau_y, \rho_x, \rho_y)$, relies on the

determination of $\hat{\Gamma}$ which is a function of the elements of $\hat{T}$ and (a, b, c). The total transmission

and reflection of the stack of layers is therefore

$$
T = |\tau_x|^2 + |\tau_y|^2, \qquad R = |\rho_x|^2 + |\rho_y|^2 \tag{1.13}
$$

1.2.4: Numerical Calculations: An Approach

The determination of the total transfer matrix of a stack (much less of a single layer) can be rather cumbersome; in most cases, one cannot determine an analytical solution for the transmission and reflection of a stack much less the transfer matrix itself. This problem can be alleviated by solving numerically. MATLAB is a suitable program for this task.

Using MATLAB, one can develop a script which considers the material parameters (z, μ, ϵ) for each layer and by way of the reduced Maxwell operator, $M(\mu, \epsilon, \vec{n})$, and Equation 1.8, one can determine the transfer matrix $\widehat{T}(M, z)$. Each transfer matrix can then be multiplied in the order they are arranged in the stack to determine the total transfer matrix for the structure (Equation 1.5). The total transfer matrix and Equation 1.11 can determine output parameters such as transmission and reflection, see Figure 1.7 for a flowchart of this process.
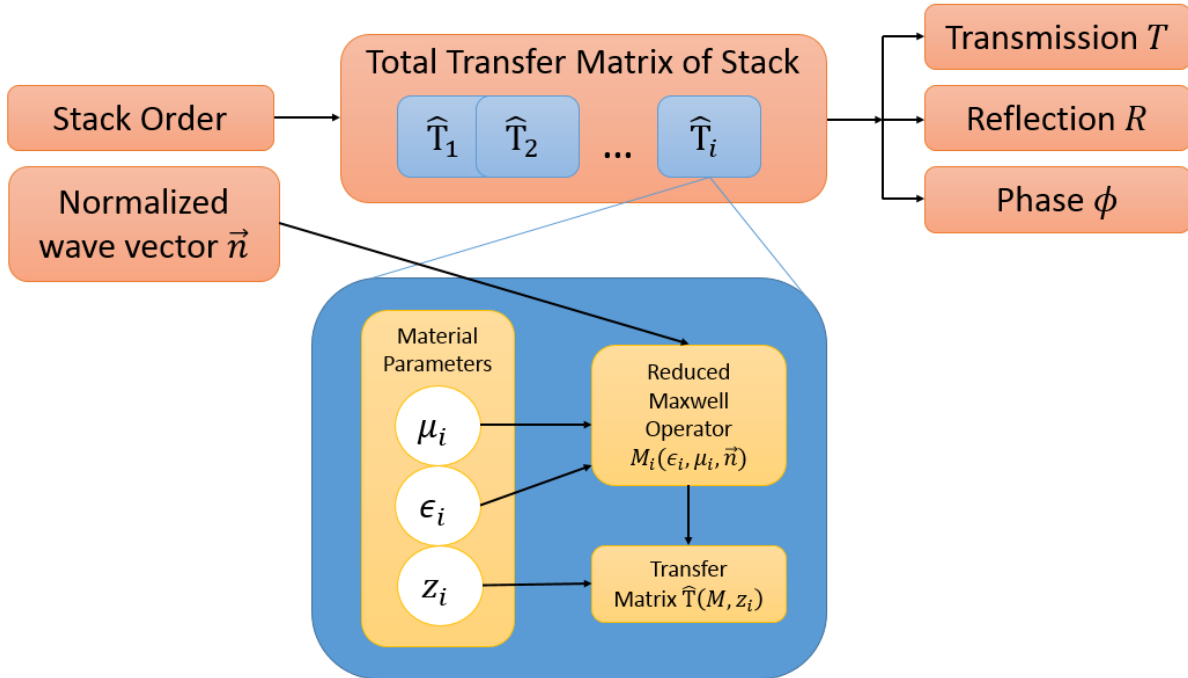
Figure 1.7 Flowchart for TM Methods

1.3: Conclusion

Up to this point, the basic nature of wave propagation through layered media has been discussed. In particular, we have established that structures with a periodic change to the refractive index will yield a characteristic transmission spectrum comprised of a photonic band gap where frequencies are rejected, and well-defined transmission peaks called Fabry-Perot resonances. We introduced the All-Dielectric Fabry-Perot Filter as a Bragg Mirror with a defect or break to the periodicity; this defect induces a characteristic transmission state inside the photonic band gap. Such a one-dimensional photonic crystal can serve as a tunable narrow band pass filter. Lastly, we discussed a numerical method capable of simulating the transmission spectrum of such structure.

CHAPTER 2: INDUCED TRANSMISSION FILTERS

2.1: Introduction

One dimensional photonic crystals with defects (See Section 1.1.2 and 1.1.3) can be designed to provide perfect transmission for a select frequency range (pass band) while rejecting all frequencies outside this range; this rejection (reflection) comes from interference between layers in the stack (See Section 1.1.2). Notwithstanding this interference, reflection is limited by the inherent transparency of the dielectric materials. The inclusion of metallic layers in such dielectric stacks has been known to provide better rejection in the photonic bandgap, albeit sometimes at the expense of diminishing transmission in the pass band; this impart is due to the intrinsic absorption of metallic layers. In particular, at microwave frequencies, stand-alone metallic films are highly reflective. This led to the development of properly designed metal-dielectric filters, known as induced transmission filters, which provide considerable transmission for a desired frequency range while rejecting all other frequencies. Primarily, this moniker refers to stacks that have been selected and arranged such that it "induces" transmission only when the incident electromagnetic wave is at a particular frequency, thus there is much literature on the careful design of such structures [5, 11, 19, 20].

In this chapter, we will show that induced transparency will occur at microwave frequencies for a metallic layer when it is embedded at the defect of a properly designed photonic structure, namely the defect photonic crystal described in section 1.1.2. Induced transmission comes from the placement of the lossy metallic layer inside the defect of the photonic structure; specifically, at the node of the localized mode produced at the defect. This induced transparency will be shown in numerical simulations by transfer matrix calculations as well as in experiment.

2.2: Numerical Setup

In simulations, the one-dimensional defect photonic crystal was organized as the following: A unit cell of dielectric layers, H and L, with dielectric constants $\epsilon_H = 9.1$ and $\epsilon_L = 1$, respectively; both layers are $4\ mm$ in thickness and have a magnetic permeability $\mu = 1$. We repeated this unit cell 7 times and added an additional H layer to the end; this will create a symmetric Bragg mirror (Section 1.1.2). A half-wave defect is then created when the central L layer is removed. This half-wave defect introduces a localized state inside the photonic bandgap, a transmission resonance. This essential design is outlined in section 1.1.3, as well as shown in Figure 2.1. Such a structure will induce transmission at the defect mode resonance when a thin metal layer is placed at its center.
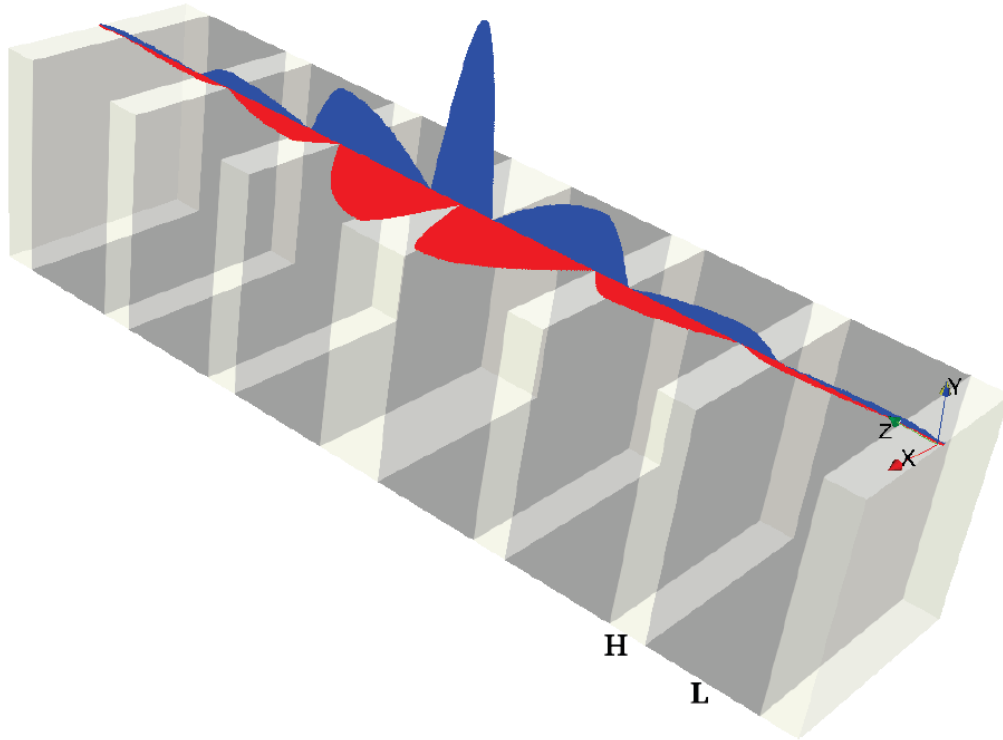
Figure 2.1 Photonic Crystal with single central defect and spatial distribution of the localized mode of electric field (red) and magnetic field (blue). At the central defect, there is a node of electric field which can be utilized to suppress conductivity losses of a metal layer when added at this location

As a matter of convention (and convenience), the same defect photonic crystal can be realized as two symmetric Bragg mirrors placed in succession. In this description, it is easy to see the structure as an all-dielectric Fabry-Perot filter where the defect becomes the spacer layer, serving as a resonating cavity. It is by this means that we designate the structure as $N:N$, where N represents the number of unit cells inside each Bragg mirror, Figure 2.1 depicts a $3:3$ structure. Despite this convention, we will also reference such structures with the notation used in Equation 1.1 where the superscripts reference the number of unit cells repeated; i.e. the $N:N$ may also be referenced as $(HL)^N HH(LH)^N$.

The nature of induced transmission through a metallic layer embedded in a defect photonic crystal comes from a non-uniform spatial distribution of the electric field, which occurs at the frequency associated with the defect mode resonance. At this frequency, the electric field is seen to have a node at the middle of the defect; this spatial profile of the electric field is seen in Figure 2.1 depicted in red. The mechanism of induced transmission comes from the placement of lossy components at the node of electric field [1]; in particular, components with losses dominated by the permittivity tensor, e.g. metallic layers. Furthermore, we note that the magnetic field amplitude in the spatial profile (in blue) is peaked at maximum at the same location as the electric field node. This means that if our metallic layer were magnetic, the magneto-optic properties could be significantly enhanced (See Chapter 4).

The metallic layer was simulated using parameters of Cobalt, which has a large and almost purely imaginary permittivity, $\epsilon_C = 4\pi i \sigma_C / \omega$ (where ω is the angular frequency, and the electric conductivity of Cobalt is $\sigma_C = 1.44 \times 10^{17} Hz$ [21]). Stand-alone metallic layers, like Cobalt, are highly reflective to microwave radiation even at thicknesses far less than the skin depth, due to

multiple reflections in the metallic layer. For example, the microwave transmittance of a Cobalt

layer of thickness of 33 nm will be on the order of 10^{-4}.

2.3: Numerical Results

The spectral response of the photonic structure of Figure 2.1 is shown in Figure 2.2. The defect in the periodic structure produces a localized electromagnetic mode at the frequency $f_0 = 7.824 \, GHz$ inside the photonic bandgap. Spatial distribution of the electric field component at resonance with the localized state, in the absence of the metallic layer F, is depicted in Figure 2.1. The intensity of the localized mode is sharply peaked at the defect position, whereas the electric field amplitude has a node, which is always the case for a high index defect. When a thin metal layer F is placed at the defect (and the node), the conductivity losses are significantly suppressed. For example, for $d = 50 \, nm$, the transmittance of the structure reduces to 0.65 at resonance, whereas in the transmission band of the photonic crystal the transmittance vanishes (Figure 2.2). At resonance, the conductivity losses depend on both the magnitude of the electric field component at the node and thickness d of the F-layer. For a given thickness d, there always exists an optimum N for minimal conductivity losses.
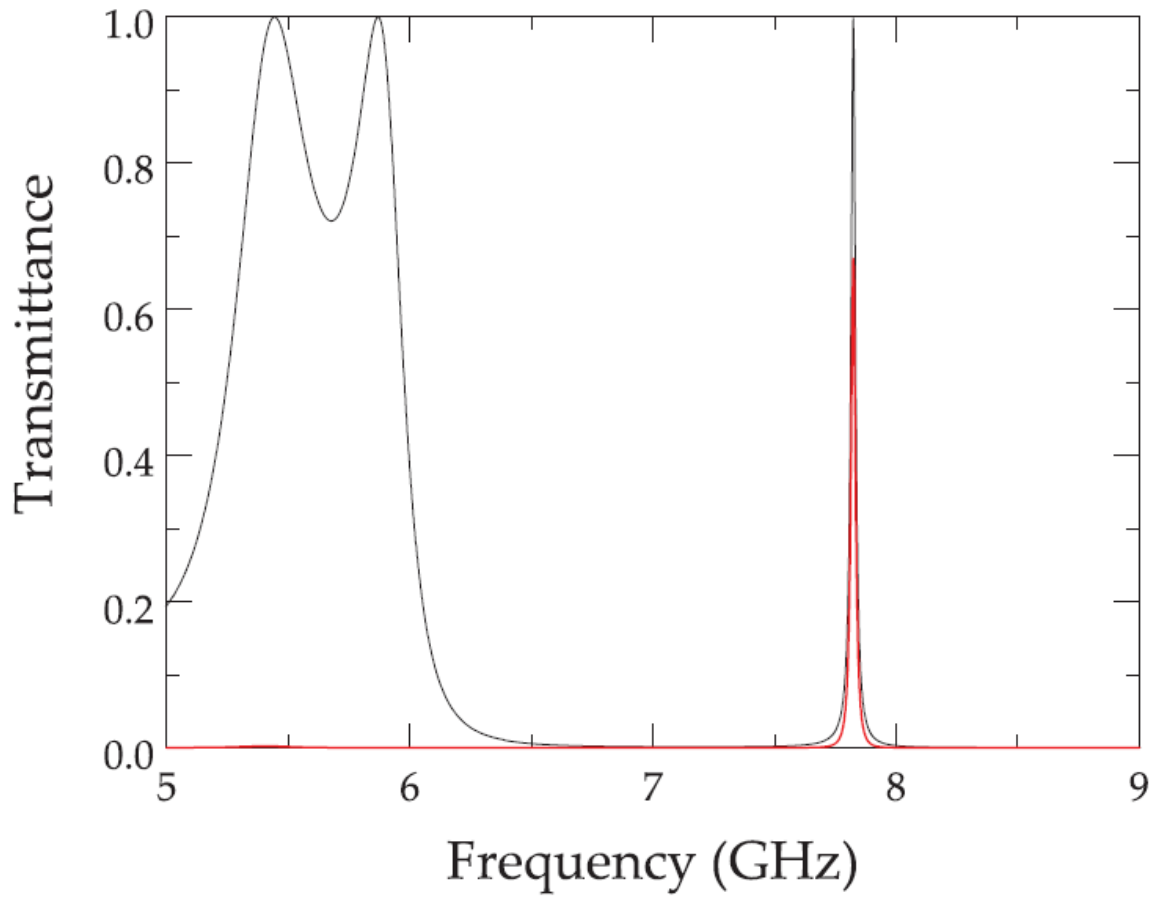
Figure 2.2 Transmittance spectra of the defect photonic crystal with metallic layer of thickness 50 nm (red) and without metallic layer F (black). The peak is at f = 7.824 GHz are due to resonant transmission via defect-induced localized states [22]

2.4: Experimental Setup

To demonstrate the phenomena of induced transmission experimentally, we fabricated a layered photonic structure of the same essential design as that in our numerical setup; we carried out transmission measurements in the microwave frequency band. The unit cell consists of a two dielectric layers, a high index ceramic layer ($\epsilon_A = 38.09 + 0.0095i$, $d_A = 1.046\ mm$) and a low index glass layer ($\epsilon_B = 3.75$, $d_B = 3\ mm$). These layers were arranged to create the $3:3$ structure. Then, at the center of the half-wave defect, a CoFe nanolayer ($d_C = 150\ nm$) was added. The CoFe was deposited on a $525\ \mu m$ glass substrate. To ensure that our 3C3 structure is symmetrical, a blank glass substrate was added to the film side of the CoFe layer to create symmetric defect.

The transmission spectrum was measured using a N5230A Agilent Network Analyzer and two microwave horn antenna. Linearly polarized microwave radiation was emitted to the structure, and transmitted signal was collected at the detector.

2.5: Experimental Results

The transmission spectrum for a single $150\ nm$ layer of CoFe on a quartz substrate (in black) is shown in Figure 2.3, the transmission of which is less than $T = -40\ dB$. When this same CoFe layer is included at the defect of our photonic structure (in red), we can obtain $T \approx -4\ dB$ transmission at resonance. This is near identical for a structure without the CoFe added (in blue). This induced transmission takes place at the defect mode frequency, $f = 9.33\ GHz$ in the spectral gap, and is associated with a localized mode whose electric field distribution places a node at the location of the CoFe. It is because of this particular spatial distribution that all conductivity losses associated with the metallic film are not seen.
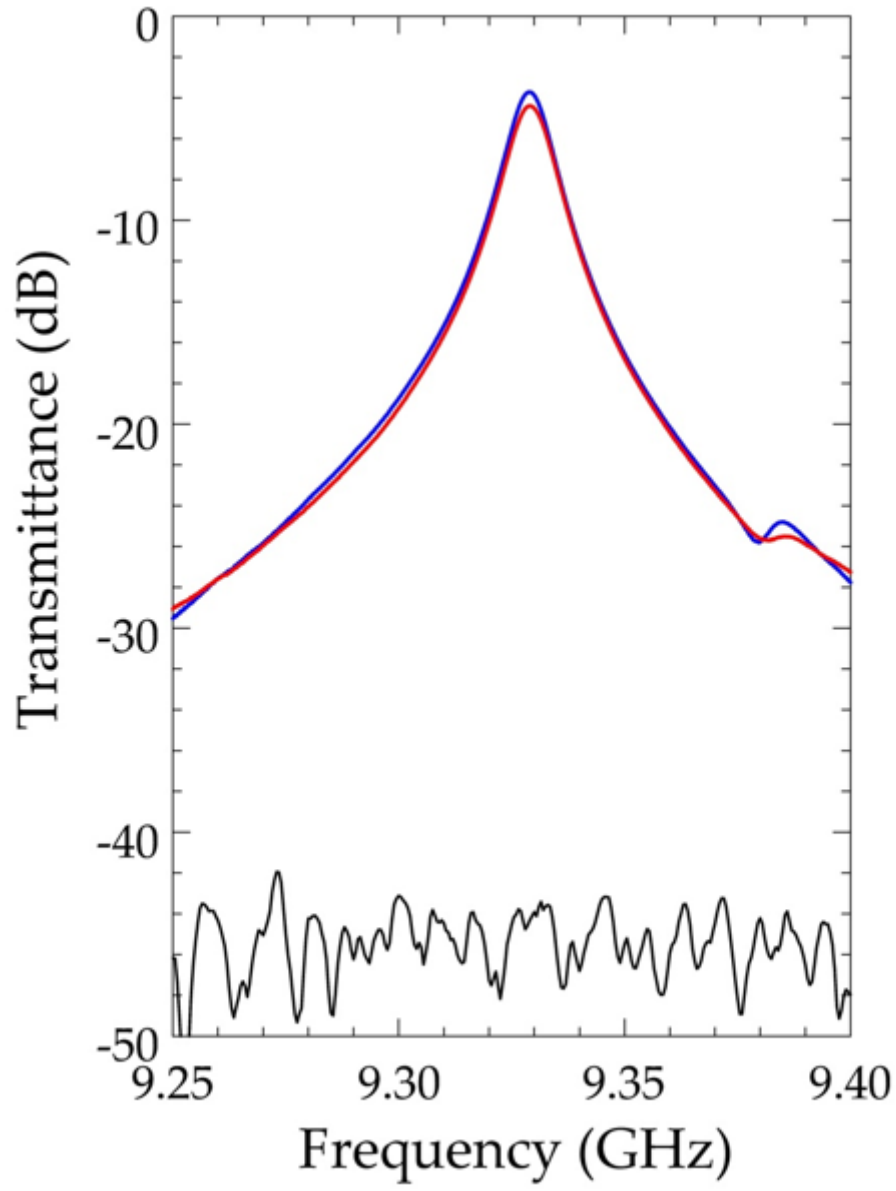
Figure 2.3 Transmission through a 150 nm thin film of CoFe, singly deposited on a quartz substrate (black) and placed in the defect photonic crystal $(HL)^3HH(LH)^3$, where H=1 mm K-38 microwave ceramic and L = 3 mm quartz layers (red). Transmission through the defect photonic crystal without CoFe is shown in blue

2.6: Conclusion

We have shown that a metallic layer exhibits induced transmission when it is placed at the node of electric field inside a properly designed photonic structure; namely, a defect photonic crystal. Any electromagnetic losses associated with the permittivity tensor of the metallic layer will be greatly suppressed when at this location.

CHAPTER 3: ASYMMETRIC METAL-DIELECTRIC PHOTONIC STRUCTURES: A CONCEPT OF REFLECTIVE POWER LIMITER

3.1: Introduction

Optical limiters are essential for protection for the human eye, optical sensors, and other sensitive devices from high power electromagnetic radiation. The basic limiter design is realized with a non-linear component whose permittivity is a function of the intensity of the incident light. When the intensity is low, the non-linear component is transparent; as the intensity of the light increases, the non-linear component become opaque. The mechanism responsible for this physical behavior can vary, e.g. two-photon absorption, heating, photoconductivity, etc. [23-25]. In all cases, the mechanism is such that the excess energy is absorbed, which in turn could lead to overheating and destruction of the device (a sacrificial limiter).

In this section, we will showcase a variation to the photonic structure described in chapter 2 as an alternative power limiter design, where the excess energy becomes reflected rather than absorbed. Specifically, this design will be modified to include a non-linear component that will change its optical thickness when the intensity of the light reaches a certain threshold; at this threshold, the photonic structure will no longer sustain a localized mode, and reflection will occur.

3.2: Theory and Setup

In Chapter 2, we introduced a one-dimensional defect photonic crystal, $N:N$, (where N is the number of unit cells in each Bragg mirror) which can induce transmission through a metallic layer when it is embedded at the node of electric field. Due to the symmetry of the structure, this node is located at the center (See Figure 2.1) and thus will only induce transmission when the metallic layer is placed exactly at the center. Once the metallic layer is placed, if one were to break this symmetry (e.g., change the optical thickness of a single layer), the node of electric field would move away from the center of the structure and no longer be at the location of the metallic layer. When the node of electric field does not coincide with the metal layer, the metal layer will have more interaction with the electric field, and a drop in transmission will occur. Specifically, at microwave frequencies and up to the far infrared, such a structure would become reflective.

To elevate our photonic structure to a reflective power limiter, we will consider modifications that break the symmetry of the current photonic structure design. Namely, the inclusion of layers that conditionally will move the node of electric field away from the metallic layer. The unique condition when the structure will induce transmission will then occur when the structure exhibits symmetry about the metallic layer. This will take place when the incident light is under a certain threshold of intensity (i.e. at the cavity, the linear and non-linear dielectric layers become degenerate) and at a particular angle of incidence (i.e., each Bragg mirror becomes degenerate).

Another perspective is to start with an asymmetric structure which supports induced transmission when the metallic layer is placed at the node of electric field of the resonance transmission mode. On the other hand, when the refractive index of one of the dielectric layers is

33

altered as a result of heating (or other non-linear process), the node of electric field is shifted from the position of the metallic layer and the structure becomes opaque.

We will consider two lossless Bragg mirrors whose respective layers are in general different. The refractive indices of the left Bragg mirror (LBM) layers are n_1 and n_2 with respective thicknesses d_1 and d_2. The refractive indices of the right Bragg mirror (RBM) layers are n_3 and n_4 with respective thicknesses d_3 and d_4. The above layers are assumed to be linear, lossless, and non-dispersive. We will engineer the constituent layers of each Bragg mirror such that for a given angle of incidence (i.e., normal incidence) the optical thickness is identical and equivalent to a quarter of some reference wavelength, i.e. $n_1 d_1 = n_2 d_2 = n_3 d_3 = n_4 d_4 = \lambda_0/4$, where $\lambda_0 = 2\pi c/\omega_0$ is the reference wavelength and $\omega_0 = 2\pi f_0$ is the angular frequency of the localized mode (c is the speed of light in vacuum and f is the frequency of the incident wave). In other words, both Bragg mirrors will be degenerate at normal incidence. For values corresponding to each dielectric layer, see Table 3.1. Each layer will be tuned to a quarter wavelength based on $f_0 = 7.5\ GHz$.

Table 3.1. APC Parameters for Dielectric Layers

	Refractive Index, n	Thickness, d (cm)
Layer 1	3.16	0.3162
Layer 2	1	1
Layer 3	4.74	0.2108
Layer 4	1.5	0.6667

The cavity consists of a left layer with refractive index n_1 and thickness d_1 and a right layer with refractive index n_4 and thickness d_4. We will replace one of the high index layers (say the left layer) at the defect with a non-linear material, thus creating an asymmetric cavity when the intensity threshold is reached. We will simulate the non-linear effect by introducing a perturbation in the permittivity; a small change $\Delta\epsilon$. When the intensity of the incident light is sufficiently low ($\Delta\epsilon \approx 0$), the non-linear layer included at the cavity will be indistinguishable from the original high index layer; thus, the photonic structure will support a localized mode. At the center, a thin metallic layer is assumed to be Cobalt with a thickness of $d_C = 180\ nm$ and the permittivity $\epsilon_C = 4\pi i\sigma_C/\omega$, where the conductivity is $\sigma = 4.31 \times 10^{16} Hz$. We will refer to our new modified photonic structure as the Asymmetric Photonic Crystal (APC).

I would like to briefly discuss the specific behavior anticipated when the APC becomes asymmetric at the defect. When degeneracy in the defect of the APC is lifted ($\Delta\epsilon > 0$), the electric field will no longer have a nodal point at the position of the defect (See Figure 3.1) which triggers various competing mechanisms. On the one hand, it will increase the impedance mismatch that the electromagnetic wave feels as it propagates inside the structure and thus enhances the reflection. At the same time, it will lead to an increase of absorption. One can estimate the effect of these two competing mechanisms to the transmission, reflection, and absorption by analyzing the transport from a single lossy δ- like defect with permittivity $\epsilon(z) = i\gamma\delta(z)$. In this case, continuity of the electric field at the point of the δ-defect and discontinuity of its derivative lead to the following expressions:

$$T_\delta = \left(\frac{2}{2+k\gamma}\right)^2, \qquad R_\delta = \left(\frac{k\gamma}{2+k\gamma}\right)^2, \qquad A_\delta = \frac{4k\gamma}{(2+k\gamma)^2} \tag{3.1}$$

Which cast light to the dual role of a lossy defect i.e. a source of increased absorption but at the same time a way to enhance reflection. An interesting feature of the above expressions in (3.1) is that the absorption is not a monotonic function of the tangent loss parameter γ. Rather it takes a maximum value $A_{max} = 0.5$ at $\gamma = 2/k$.

The second mechanism is subtler and it occurs only for the case of resonant transport. In this case, the bulk losses due to the strong interaction of the electric field with the metallic layer compete with the losses due to the leakage from the boundaries of the total structure. The former is proportional to $|E|^2$, i.e. the field intensity at the position of the lossy defect while the latter depend on the coupling of the resonant mode to the free space via the boundary of the composite structure. As the permittivity change $\Delta\epsilon$ increases, the bulk losses overrun the losses due to the boundary leakage (which remain constant) and eventually spoil the resonance (see red electric field profile in Figure 3.1). Thus photons do not dwell in the resonant mode and therefore cannot be absorbed by the metallic layer i.e., the absorption A at the resonance frequency f_0 diminishes while the reflection becomes the dominant effect, i.e. $R = 1$, and $T = 0$.

3.3: Results

Numerical simulations using transfer matrix methods (see Section 1.2) were done for the Asymmetric Photonic Crystal (APC) with 5 unit cells in each Bragg mirror (a $5:5$ structure). The $5:5$ APC is depicted in the left panel of Figure 3.1 with the spatial distribution of the unperturbed and perturbed state superimposed. For the unperturbed state (in blue), the APC supports a localized mode with a node of electric field located at the center of the structure; this node can be seen in a logarithmic plot on the upper panel of Figure 3.1 where the metallic layer is show in green. Because this node of electric field coincides with the metal layer, the APC will exhibit a transmission resonance $T \approx 1$ (See Figure 3.1, lower right panel in blue) at the frequency f_0.
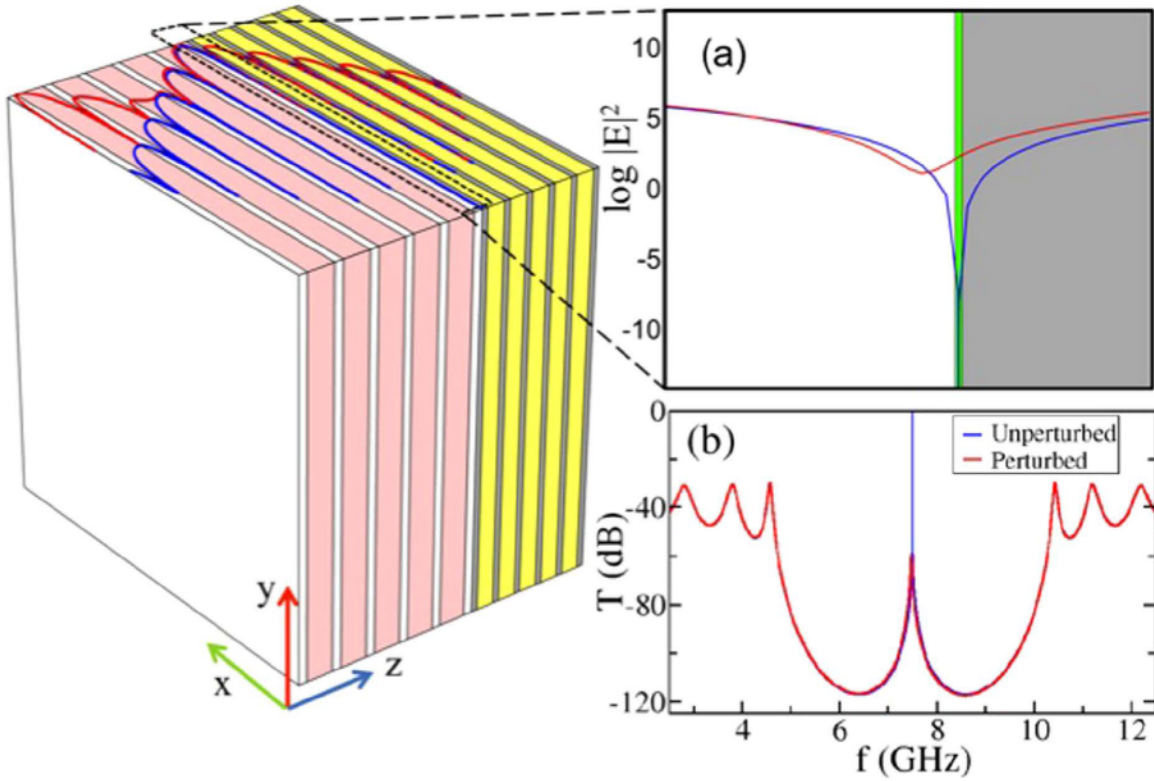
Figure 3.1 The Asymmetric Photonic Crystal (APC)

For the perturbed state (in red), specifically with a 2% increase in the permittivity, the APC becomes asymmetric and the node of electric field moves away from the center of the structure (upper right panel). Because of this, there is a stronger electric field interaction with the metal and thus a strong reduction in transmission in the form of reflection (lower right panel in red).
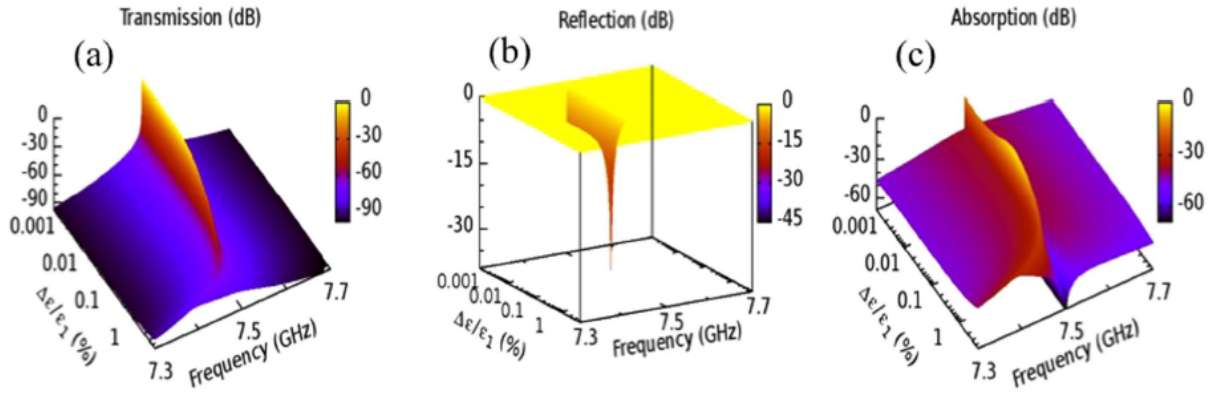
Figure 3.2 APC Transmission, Reflection, and Absorption

In Figure 3.2, we expand on the transmission T, reflection R, and absorption A of the APC with 3D plots versus frequency and perturbation $\Delta\epsilon$. The numerical data are in perfect agreement with the theoretical expectations discussed above. Specifically, we find that again for the unperturbed state ($\Delta\epsilon \approx 0$), the transmission at resonance frequency is almost unity $T(f_0) \approx 1$ (Figure 3.2a) while the associated reflection and absorption are zero i.e. $R \approx 0$, and $A \approx 0$ respectively (Figures 3.2b,c). As we increase the perturbation, the absorption initially increases (see peak at $\Delta\epsilon \sim 0.05\%$) but as $\Delta\epsilon \geq 1\%$ it starts decreasing reaching values as low as $A = -40 \ dB$. For even larger permittivity changes, the structure becomes completely reflective (See Figure 3.2b). The small red shift of the resonance f_0 as $\Delta\epsilon$ increases is due to the increase of the

effective index of refraction $n_{eff} = \sqrt{\epsilon_2 + \Delta\epsilon}$ of the defect layer which (for constant defect width), in turn, leads to an increase of the resonance wavelength $\lambda_0 = 2\pi c/\omega_0$ such that $2d_2 = \frac{\lambda_0}{2n_{eff}}$. This same effect is also seen in Figure 3.1, slightly shifting the resonance frequency in the perturbed state to $f_0 = 7.46\ GHz$.

3.4: Chapter Conclusion

In numerical simulations, we have shown that an asymmetric one-dimensional photonic structure with an added metallic layer can serve as an effective reflective power limiter. In conjunction with the induced transmission discussed in Chapter 2, a break in symmetry to the structure can render the structure completely reflective, thus removing the induced transmission. In this chapter, we discussed that the use of a non-linear component, i.e. one that changes its permittivity with an increase in light intensity, causes the nodal point of electric field to move away from the location of the metallic layer, causing more electric field interaction and thus an essential decrease in transmission. Unlike standard passive limiters, when the non-linear component is at the limiting threshold, the mechanism which decreases the transmission is not absorptive, but reflective; thus this design would not have any potential to overheat (and self-destructive). Such a structure thus is far more sustainable for commercial use.

CHAPTER 4: ENHANCEMENT OF FARADAY ROTATION IN MAGNETIC METAL-

DIELECTRIC PHOTONIC STRUCTURES

4.1: Chapter Introduction

Up to this point, we have discussed metal-dielectric photonic structures that are capable of high transmission due to a non-uniform electromagnetic spatial distribution. We will now show that the defect mode resonance that generates this particular spatial distribution is also capable of enhancing magneto-optical properties [22]. Such a photonic structure would enable the use of ferromagnetic metals, which have tremendous magnetic properties but are often shunned due to conductivity losses.

The importance of magnetic materials in optics and microwave engineering [26, 27] comes mainly from their nonreciprocal properties: properties with which a wave's transmission and phase become altered after the direction of propagation is reversed. For example, magnetic circular birefringence and circular dichroism provide a nonreciprocal differential phase shift and attenuation, respectively; a by-product of this is the magnetic Faraday Effect. Such phenomena and their associated magnetic components thus are integral in nonreciprocal devices such as isolators, circulators, modulators, etc. Although nonreciprocal devices can be realized from magnetic materials, bulk magnetic materials are often not appropriate when incorporating these devices into integrated circuits. Therefore, one must employ certain miniaturization techniques where components are reduced in size, but maintain effectiveness. Furthermore, there are additional limitations due to the absorption associated with magnetic materials. Many magnetic materials with otherwise perfect physical characteristics have been rejected because of strong losses in a given frequency range of interest (ferromagnetic metals). Indeed, ferrites have

become ubiquitous among nonreciprocal devices, however ferrites are often quite expensive and too bulky for high performance designs.

The absorption suppression mechanism in Ref. [1] provides a selective enhancement technique that can be used to suppress the electric losses in ferromagnetic metals while enhancing the more desirable light matter interactions, such as Faraday rotation (This technique can already be realized from structures like that described in Chapter 2). Furthermore, in the microwave regime, there is more control over the magnetic interaction by magnetic field due to the presence of the ferromagnetic resonance: a phenomenon where there is absorption of electromagnetic energy through the precession of magnetic moments. With a structure that is can obtain high transmission and enhanced nonreciprocal properties through a ferromagnetic metal, one can tune an applied magnetic field (by intervention of the ferromagnetic resonance) to achieve large Faraday rotation such as 45°; such is necessary for standard commercial isolators.

In this chapter, we will showcase a metal dielectric photonic structure that is capable of induced transmission as well as enhanced nonreciprocal properties, namely Faraday rotation. In conjunction with the discussion in chapter 2 and 3, Such a structure will be realized as a omni-directional microwave isolator: a one-way device that transmits light in only one specific direction. The organization of this chapter is the following: We will first provide a description of the magnetic permeability of a ferromagnet. Through this we will discuss ferromagnetic resonance, Faraday rotation, and briefly illustrate how such a component can act as a rotator: a vital part to the isolator design. Then, we will showcase the photonic structure itself as a omni-directional microwave isolator through the intervention of Ref. [1]. Lastly, we will highlight that our photonic structure can create a mini-band of high transmission with Faraday rotation when coupled to a succession of identical structures.

4.2: Ferromagnetism

4.2.1: Introduction

Ferromagnetism refers to a strong type of paramagnetism in which atomic magnetic dipoles, associated with the spin of unpaired electrons, maintain their alignment after an outside applied magnetic field is removed. This tendency to retain magnetization comes from the interaction of nearby dipoles which generates domains or sections where all magnetic moments are aligned. The net magnetization is therefore related to the total sum of magnetic moments in all domains and can be altered with an applied magnetic field [28].

When a ferromagnet is irradiated with electromagnetic waves (alternating magnetic field), the magnetic susceptibility of the ferromagnet is found to exhibit resonant behavior for particular frequencies. Namely, the ferromagnetic resonance, which is a condition of maximum absorption in electromagnetic energy based on a static magnetic field. This phenomenon is polarization dependent and nonreciprocal.

In this chapter, we will derive the ferromagnetic resonance from the equation of motion of magnetization for a ferromagnet. We will consider first a lossless interaction between magnetization and applied magnetic field, then assume magnetic losses; we will also briefly discuss other considerations such as shape anisotropy. After this discussion, we will briefly describe the nature of Faraday rotation and the isolator design

4.2.2: The Equation of Motion of Magnetization

To describe the behavior of the magnetization of a ferromagnet, we will consider the

equation of motion of magnetization proposed by Landau and Lifshitz in 1935 [29].

$$\frac{\partial \vec{M}}{\partial t} = -\gamma \vec{M} \times \vec{H}$$
(4.1)

where γ is the gyromagnetic ratio, M is the magnetization, and H is the magnetic field. In this

equation, magnetic moments are considered as classical tops, and thus we make an equivalence

between torque (right-hand side) and the change of angular momentum with respect to time (left-

hand side). The negative sign as well as the gyromagnetic ratio both arise from the quantum-

mechanical relation between the spin of magnetic moment and the angular momentum of an

electron. However, in the classical theory, the value of the gyromagnetic ratio is no longer

influenced by the spin of the electron alone, but instead also the orbital magnetic moment

interaction. Thus values of the gyromagnetic ratio are often found from experiment for each

ferromagnet [30-32]. More on this description can be found in the text by Gurevich [33].

4.2.3: The μ Tensor

When a ferromagnet is under the influence of a magnetic field, the behavior of the

magnetization can be described by the equation of motion of magnetization. When this magnetic

field consists both of a static term as well as an alternating term, the results best describe the

behavior of the magnetization when under the influence of a static magnetic field as well as

electromagnetic radiation. We consider the sum of the static and alternating parts for both the

magnetic field and the magnetization

$$\vec{H} = \vec{H}_0 + \vec{h}_\sim, \qquad \vec{M} = \vec{M}_0 + \vec{m}_\sim \tag{4.2}$$

The upper case terms, $\vec{H}_0$ and $\vec{M}_0$, refer to the static magnetic field and magnetization,

respectively. The lower case terms, $\vec{h}_\sim$ and $\vec{m}_\sim$, refer to the alternating parts of the magnetic field

and magnetization, respectively. Each alternating term is assumed to be harmonically time

dependent with a frequency ω and is assumed to be much smaller than its static counterpart.

Using the complex variables approach, we can define the alternating parts as complex

exponentials. Substituting (4.2) into (4.1) where the alternating terms have the following form:

$$\vec{h}_\sim = \vec{h}\exp(i\omega t), \qquad \vec{m}_\sim = \vec{m}\exp(i\omega t) \tag{4.3}$$

The real parts of both equations being the true equivalence. With a few considerations [33],

substituting (4.2) into (4.1) will yield a linearization of the equation of motion.

$$\frac{\partial \vec{m}_\sim}{\partial t} + \gamma \vec{m}_\sim \times \vec{H}_0 = -\gamma \vec{M}_0 \times \vec{h}_\sim \tag{4.4}$$

The complex amplitudes of the vectors $\vec{h}_\sim$ and $\vec{m}_\sim$ both satisfy (4.4), which can be projected

onto the axes of a Cartesian coordinate system with the z axis coinciding with the direction of H_0

45

and M_0. The solution of which defines the magnetic susceptibility, $\overleftrightarrow{\chi}$, first obtained by Polder [34]:

$$\vec{m} = \overleftrightarrow{\chi}\,\vec{h} \tag{4.5}$$

This magnetic susceptibility, $\overleftrightarrow{\chi}$, is a non-symmetric second-rank tensor:

$$\overleftrightarrow{\chi} = \begin{bmatrix} \chi & i\chi_a & 0 \\ -i\chi_a & \chi & 0 \\ 0 & 0 & 0 \end{bmatrix} \tag{4.6}$$

With values

$$\chi = \frac{\gamma M_0 \omega_H}{\omega_H^2 - \omega^2}, \qquad \chi_a = \frac{\gamma M_0 \omega}{\omega_H^2 - \omega^2} \tag{4.7}$$

And

$$\omega_H = \gamma H_0 \tag{4.8}$$

The components of the magnetic susceptibility tensor (4.7) are defined for an isotropic lossless ferromagnet, magnetized to saturation. The presence of the off-diagonal elements in the magnetic susceptibility imply that the transverse components of the AC magnetic field, $\vec{h}$, will excite the AC magnetization components, $\vec{m}$, both parallel and perpendicular to it. Furthermore, the presence of the factor i is indicative of a phase shift by $\frac{\pi}{2}$. This type of non-symmetry is referred to as *gyrotropy*. This same type of gyrotropy also exists for electric susceptibility in the presence of a static magnetic field which leads to Faraday and Kerr effects at optical frequencies [35]. In the case of magnetic susceptibility containing these components, we may refer to such effects as magnetic. In ferromagnets, this behavior dominates at microwave and far infrared frequencies.

The frequency dependence of the components of the magnetic susceptibility tensor relates to a pole between the frequency and static magnetic field. This singularity is defined by equation (4.8). The phenomenon that results from satisfying equation (4.8) is called the *ferromagnetic resonance*. When this condition is met, the ferromagnet exhibits maximal absorption of electromagnetic energy. Classical models of the ferromagnetic resonance were first illustrated by Arkad'yev [36] in 1912, and initial quantum based models by Dorfmann [37] in 1923. However, these models were incomplete as the spin as well as ferromagnetism wasn't fully explained until 1928. It wasn't until 1935 that a more correct understanding was proposed by Landau and Lifshiftz [38] and later experimentally discovered by Griffiths in 1946 [39].

The nature of the ferromagnetic resonance becomes more interesting with further inspection of the magnetic susceptibility in (4.6). Considering the transverse components of the AC magnetic field and AC magnetization, the follow results can be found after diagonalization of (4.6)

$$m_\pm = \chi_\pm h_\pm \tag{4.9}$$

Where

$$h_\pm = h_x \pm i h_y, \qquad m_\pm = m_x \pm i m_y \tag{4.10}$$

The equations in (4.10) define the eigen-polarizations of the ferromagnet and are representative of an electromagnetic wave with a circular polarization. Circular polarization is a special case of elliptical polarization where the transverse components of the electromagnetic wave maintain amplitude but change direction in a rotary manner about the propagation direction, thus tracing a circle. The circular components, $h_\pm$ and $m_\pm$, both map to one another by

47

the expression in (4.9) with the corresponding circular components of the magnetic

susceptibility, $\chi_\pm$ defined as:

$$\chi_\pm = \chi \pm \chi_a = \frac{\gamma M_0}{\omega_H \mp \omega} \qquad (4.11)$$

In this form, it is clear that only the χ_+ will exhibit resonant behavior as it is the only expression

with a pole; thus only one polarization will exhibit resonant behavior. With the equations in (4.7)

and (4.11), we can now define a similar expression for the magnetic permeability.

$$\overleftrightarrow{\mu} = \overleftrightarrow{I} + 4\pi\overleftrightarrow{\chi} = \begin{bmatrix} \mu & i\mu_a & 0 \\ -i\mu_a & \mu & 0 \\ 0 & 0 & 1 \end{bmatrix} \qquad (4.12)$$

(Where $\overleftrightarrow{I}$ is the identity matrix) The elements of the permeability or μ tensor are:

$$\mu = 1 + 4\pi\chi = \frac{\omega_H(\omega_H + \omega_M) - \omega^2}{\omega_H^2 - \omega^2}, \qquad \mu_a = 4\pi\chi_a = \frac{\omega\omega_M}{\omega_H^2 - \omega^2} \qquad (4.13)$$

Where

$$\omega_M = 4\pi\gamma M_0 \qquad (4.14)$$

As one would expect, we can also diagonalize the permeability tensor and again obtain circular

components as solutions for diagonalization.

$$\mu_\pm = 1 + 4\pi\chi_\pm = \mu \pm \mu_a = \frac{\omega_H + \omega_M \mp \omega}{\omega_H \mp \omega} \qquad (4.15)$$

The magnetic permeability, like the magnetic susceptibility, exhibits a singularity only in one of

its circular components. Again, only one circular polarization will exhibit resonant behavior.

4.2.4: Magnetic Losses & Shape Anisotropy

In the previous section, we derived the expression for ferromagnetic resonance for a lossless ferromagnet magnetized to saturation. In this section we will now consider magnetic losses. The oscillations of magnetization resulting from equation (4.1) and reflected in equation (4.12) are inevitably accompanied by dissipation of magnetic energy [38]. These magnetic losses can be accounted for by replacing the real frequency ω with a complex quantity $\omega' + i\omega''$. This will result in the appearance of imaginary terms in (4.7) and consequently (4.13). A more formal approach however would be to include a loss term in the equation of motion of magnetization (4.1) as proposed by Gilbert [40]:

$$\frac{\partial \vec{M}}{\partial t} = -\gamma \vec{M} \times \vec{H} + \frac{\alpha}{|M|} \vec{M} \times \frac{\partial \vec{M}}{\partial t} \tag{4.16}$$

When the dissipation parameter α is considered small, linearization of (4.16) will arrive at the same magnetic permeability tensor as (4.12), but with the following consideration:

$$\omega_H \rightarrow \omega_H + i\alpha\omega \tag{4.17}$$

Furthermore, the presence of losses will generate a longitudinal term, however this term is of no consequence when considering transverse AC magnetic fields (or electromagnetic radiation propagating along the z axis). The effect of losses subtly alters the ferromagnetic resonance condition to include the dissipation parameter

$$\omega = \frac{\omega_H}{1 + \alpha^2} \tag{4.18}$$

In most cases, the dissipation parameter for materials is less than unity and thus will have only a minor effect on the ferromagnetic resonances condition.

After equation (4.17) is applied to equation (4.6) and (4.7), the components of the magnetic

susceptibility will become complex, the real and imaginary parts of the components of the

magnetic susceptibility can be found in the left panel of Figure 4.1. When this same magnetic

susceptibility is diagonalized, we again will only resonant behavior in one of the components.

This is evident in the right panel of Figure 4.1.
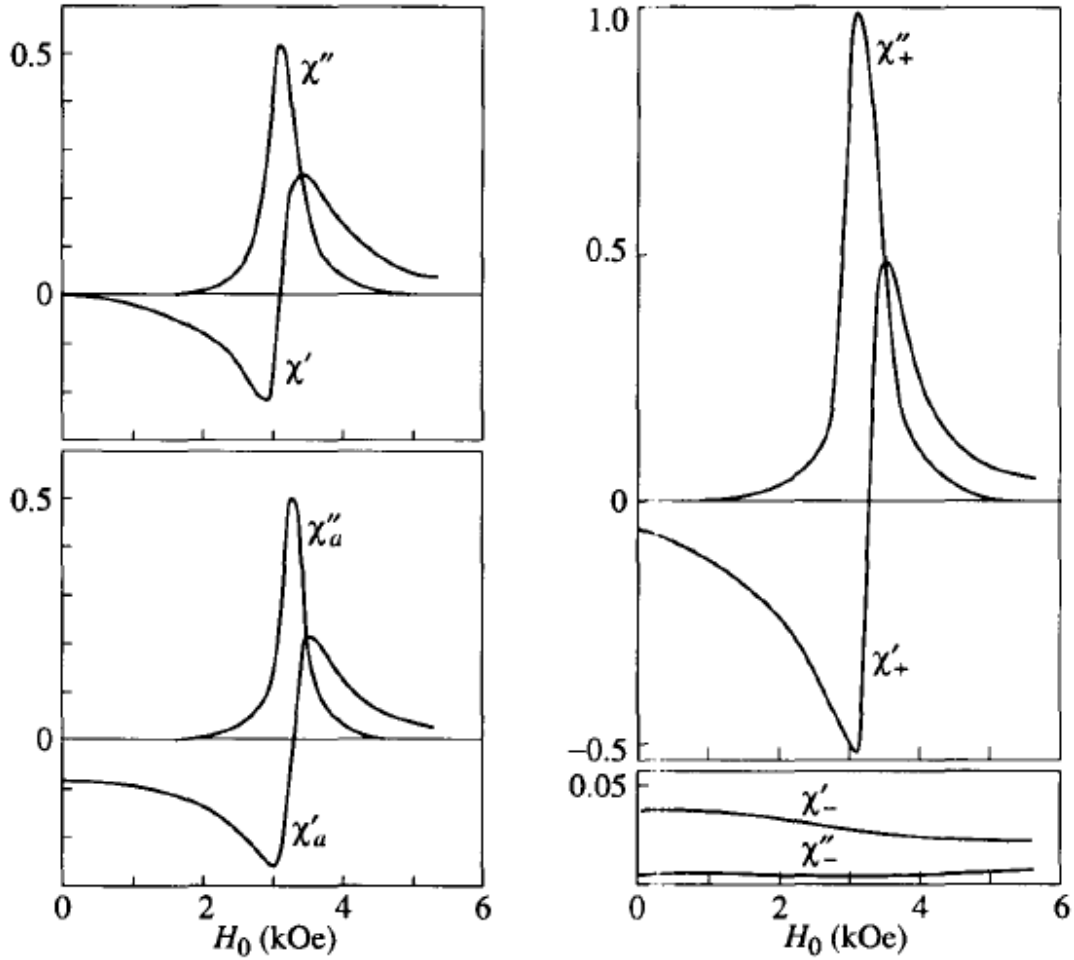
Figure 4.1: Real and Imaginary Parts of the Magnetic Susceptibility Tensor. This was calculated using $M_0 = 160\ G$, $f = 9.4\ GHz$, and $\alpha = 0.025$.

Up to this point, we have not considered the boundaries of the ferromagnetic sample and the effect it would have on the applied magnetic field in (4.8). When considering a ferromagnetic sample in the presence of an external magnetic field, a demagnetizing field resulting from the bound currents will also appear. This demagnetizing field will be related to the magnetization of the sample as well as the shape:

$$\vec{H} = \vec{H}_e - \overleftrightarrow{N}\vec{M} \tag{4.19}$$

The second term in (4.19) is the demagnetizing field. The tensor $\overleftrightarrow{N}$ is referred to as the demagnetizing tensor and is directly related to the shape of the sample. The expression in (4.19) is only true for ellipsoidal samples [41].

The results of including this demagnetizing field of an ellipsoidal sample will lead to another transformation (similar to when we included losses). For this research, ferromagnetic samples will be considered as infinitely thin plates with a total magnetization saturated along the z direction, coinciding with the external magnetic field direction. This consideration will yield a demagnetizing tensor with only a single term on the diagonal [33].

$$\overleftrightarrow{N} = \begin{bmatrix} 0 & 0 & 0 \\ 0 & 0 & 0 \\ 0 & 0 & 4\pi \end{bmatrix} \tag{4.20}$$

With regard to other forms of anisotropy (such as crystalline or magnetic) [42], the effect ultimately will be additive that in equation (4.19) although some considerations can be more involved.

4.2.5: Faraday Rotation

Faraday rotation (or the Faraday effect) refers to the rotation of the plane of polarization that occurs when light travels through a material under the influence of an applied magnetic field. The origin of this phenomenon is gyrotropic in nature and stims from a non-degenerate interaction of circular polarization with the magnetic material. Specifically, a differential phase shift between circular polarizations; such a property is called circular birefringence. Because a linearly polarized wave can be decomposed into left and right-handed circularly polarized waves, the circular birefringence that occurs when a wave travels through the magnetic material manifests itself in the form of a rotation of the plane of polarization (The same effect takes place for reflected waves, this phenomenon is known as the Kerr effect or Kerr rotation).

For a ferromagnetic material that is in the vicinity of the ferromagnetic resonance (that is ω approaches ω_H), large Faraday rotation can occur. This rotation comes from a differential phase shift between circular polarizations. This difference in circular components can be seen in the magnetic susceptibilities in the right panel of Figure 4.1. As we approach the ferromagnetic resonance condition, this difference will increase and thus increase the Faraday rotation. However, as one gets close to the condition of ferromagnetic resonance ($\omega \approx \omega_H$), the imaginary component of the more interacting circular component (χ''_+) will begin to peak and maximum absorption will take place for one of the circular components; this property is called circular dichroism. Therefore, with the use of ferromagnetic resonance as a method for increasing Faraday rotation, one must remain in the vicinity of the resonance condition of equation (4.18) where nonreciprocal differential phase shift (circular birefringence) remains dominate over nonreciprocal differential attenuation (circular dichroism).

4.2.6: The Isolator Design

Here we will briefly explain the isolator design [28, 43]. A standard commercial isolator (See Figure 4.2) consists of a two polarizers on either side of a rotator; the rotator provided 45° Faraday rotation. Thus, when a linearly polarized wave is incident on the rotator (illustrated by (1) in Figure 4.2), the exiting wave will be near identical but with the plane of polarization rotated by 45° (illustrated by (2) in Figure 4.2). The polarizers each have the same orientation as the entering and exiting waves (same as (1) and (2)). When a wave travels from the reverse side, the wave will automatically be at a 45° angle due to the polarizer, then the rotator will rotate the polarization another 45° in the same orientation as it did going forward through the rotator; thus yielding a total 90° rotation of the plane of polarization (illustrated by (3) in Figure 4.2). This will cross with the polarizer at the front of the rotator and prevent any backward transmission.
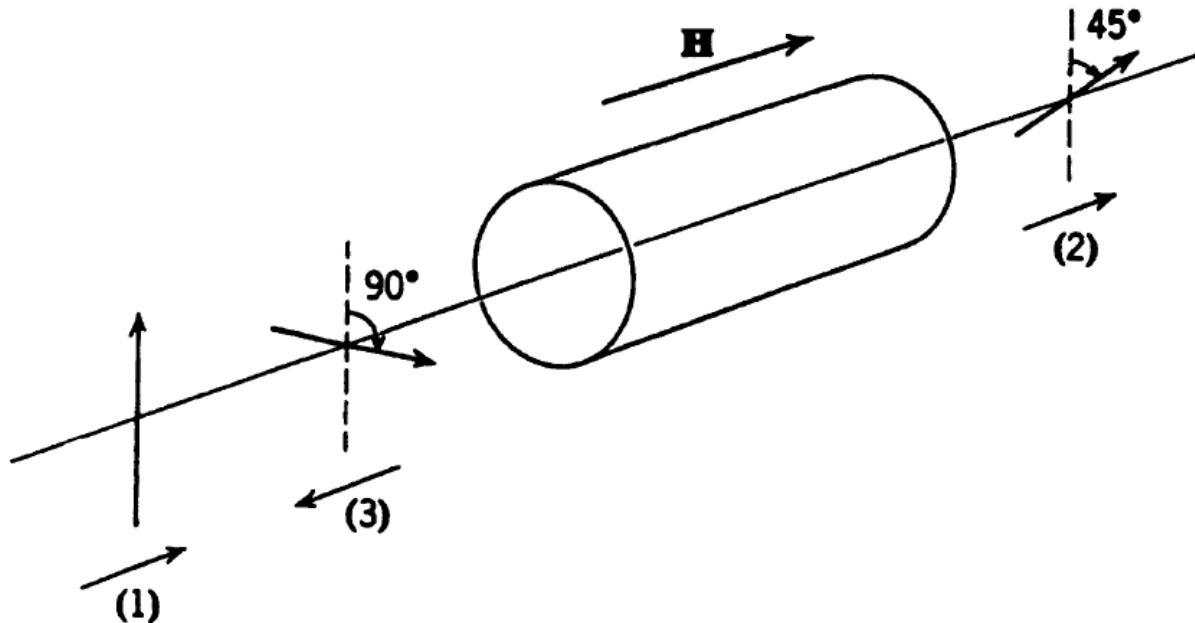
Figure 4.2: Schematic of Basic Isolator.

The cornerstone of the isolator design lies with the nonreciprocity of the rotator. The reciprocity of a rotator refers to its invariance under time reversal. Since the initial wave, traveling from (1) to (2), will rotate clockwise for the prospective of the source, time reversal would suggest that a wave traveling from (2) to (1) would thus rotate counter-clockwise, however this is not the case and the rotation remains clockwise (It is also important to mention that magnetic field is a pseudo-vector which gains a sign change upon reflection). For a propagating wave, time reversal is identical to a wave traveling in the opposite direction, thus from (2) to (1). Therefore, it is intuitive that a one-way device can be realized from nonreciprocal components like the rotator.

4.2.7: Conclusion

In this section, we have provided a derivation of ferromagnetic resonance for a lossless and lossy ferromagnet that has been magnetized to saturation. We discussed that this ferromagnetic resonance only takes place for one of two circular polarizations. In general, this difference between circular polarization interaction can lead to circular birefringence and dichroism where the former can cause Faraday rotation, a rotation of the plane of polarization. Magnetic materials with such properties are vital components in isolators.

4.3: Microwave Isolator

4.3.1: Introduction

One-way devices are essential components in a microwave (MW) network. They are especially used in the protection of sources from unwanted reflection. One such device is the MW isolator (See Section 4.26), whose function stems from the nonreciprocal properties of constituent magnetic materials; namely, a magnetically induced rotation of the plane of polarization – Faraday rotation (See section 4.25). Though nonreciprocal devices (such as isolators, circulators, modulators, etc.) can be realized from magnetic materials, bulk magnetic materials are often not appropriate when incorporating these devices into integrated circuits. Therefore, one must employ certain miniaturization techniques where components are reduced in size, but maintain effectiveness. Furthermore, there are additional limitations due to the absorption associated with magnetic materials. Many magnetic materials with otherwise perfect physical characteristics have been rejected because of strong losses in a given frequency range of interest. Such is true for ferromagnetic metals.

In the context of integrated circuits, much research has been done in the miniaturization of optical components (such as nonreciprocal devices) to develop hybrid optoelectronic circuits as well as purely photonic circuits that can provide significant improvement over conventional electronic circuits. In particular, photonic crystals (See Chapters 1 and 2) have championed the field of integrated photonics and revolutionized the realm of telecommunications. Photonic structures (such as our $3:3$ structure in Chapter 2) can localize light in the vicinity of defects and can provide high transmission and even enhance properties of its constituents [44, 45]. Indeed, photonic structures with magnetic components have shown such enhancement of nonreciprocal properties [46, 47].

There have been major developments in magneto-photonic crystals that display enhanced nonreciprocal properties [48], such as the magnetic Faraday Effect. Indeed, a noticeable enhancement of Faraday rotation was observed in magnetic thin-film layers sandwiched between Bragg reflectors [49-51], periodic multilayers, and other structures supporting slow and localized modes [52-54]. Such structures are encouraged as miniaturization solutions since the magneto-optic response is far superior to uniform bulk magnetic materials. However, in these cases the Faraday rotation enhancement was accompanied by a significant decrease in the optical transmittance. Although the transmittance can be somewhat improved by minimizing the reflectance of the photonic structures [55, 56], the output can still be severely affected by absorption losses [57, 58]. This limitation stems from the fact that at optical frequencies, both the nonreciprocal response and photon absorption are governed by the permittivity tensor (ϵ) of the magnetic material. Thus, any enhancement of the nonreciprocal response, such as the Faraday effect, is inevitably accompanied by enhancement of absorption losses. Such structures thus can only be effective with low-loss magnetic materials, such as ferrites, while completely avoiding magnetic metals such as ferromagnets.

In Chapter 2, we discussed that absorption by lossy components in one-dimensional photonic crystals can be greatly suppressed by means of induced transmission [1, 11, 19] (See Chapter 2). This absorption suppression mechanism was due to a highly non-uniform electromagnetic field distribution inside the photonic crystal. For example, at the transmission resonance, the electromagnetic field in the crystal is nearly a standing wave comprising a pair of counter propagation Bloch waves, so that the nodes of the electric field component coincide with the antinodes of the magnetic field component and vice versa. When components with losses dominated by the permittivity tensor (ϵ), e.g., metallic components, are positioned at a node of

the electric field, their absorption is greatly suppressed. Therefore, the nonreciprocal properties should be dominated by the magnetic permeability tensor in order for there to be any enhancement in nonreciprocal properties. In ferromagnets, this is the case at microwave and far infrared frequencies.

In this chapter, we will discuss how the use of the absorption suppression mechanism can induce transmission while simultaneously enhanced the nonreciprocal properties of an embedded metallic layer when that layer is a ferromagnetic metal. Specifically, we will show how the defect photonic structure from Chapter 2 can be used to obtain high transmission and 45° Faraday rotation. This will be shown though numerical simulations. Additionally, we will also discuss the effectiveness of the single defect design for higher N Bragg mirror, and expand on the effective frequency range by considering a super-lattice of magneto-photonic structures where weakly coupled resonators can have lifted degeneracy between high Q resonances thus increasing the bandwidth.

4.3.2: Numerical Setup & Methods

We consider again the essential defect photonic structure from Chapter 2 but with different materials. The 1-D MW photonic crystal consists of layers of alumina (H) and air (L) of dielectric constants $\epsilon_H = 10$ and $\epsilon_L = 1$, respectively, and magnetic permeability $\mu = 1$. Since alumina and air have negligible absorbing at MW frequencies, we take them to be lossless in our numerical simulations. The dielectric layers have quarter-wave thicknesses $d_j = \lambda_0/\left(4\sqrt{\epsilon_j}\right)$, for $j = H, L$, at the wavelength $\lambda_0 = 4\ cm$ corresponding to the midgap frequency $f_0 = 7.5$ GHz of the quarter-wavelength layer stack. Starting with a period stack $HLH \dots L$ of $M = 2N + 1$ unit cells (N is a positive integer), we add layer H at the end of the stack and remove the middle layer L, to construct a symmetric layer stack with a central half-wave defect. The resulting structure is designated $N{:}N$ (The top panel of Figure 4.3 depicts a $3{:}3$ structure).

The half-wave defect introduces a pair of polarization-degenerate localized states at the mid-gap frequency f_0. The spatial profiles of the electric and magnetic field amplitudes of the localized mode of the $3{:}3$ structure are shown in Fig 4.3. Whereas the electric field is seen to have a node at the middle of the defect, the magnetic field is sharply peaked at the same position. The magneto-photonic structure NCN is then constructed by inserting a cobalt (C) layer in the node of the electric field at the middle of the defect. We also consider periodic arrangements with multiple defects ($N{:}M{:}N$, $N{:}M{:}M{:}N$, etc.) and multiple cobalt layers ($NCMCN$, $NCMCMCN$, etc.) (See Section 4.3.4).
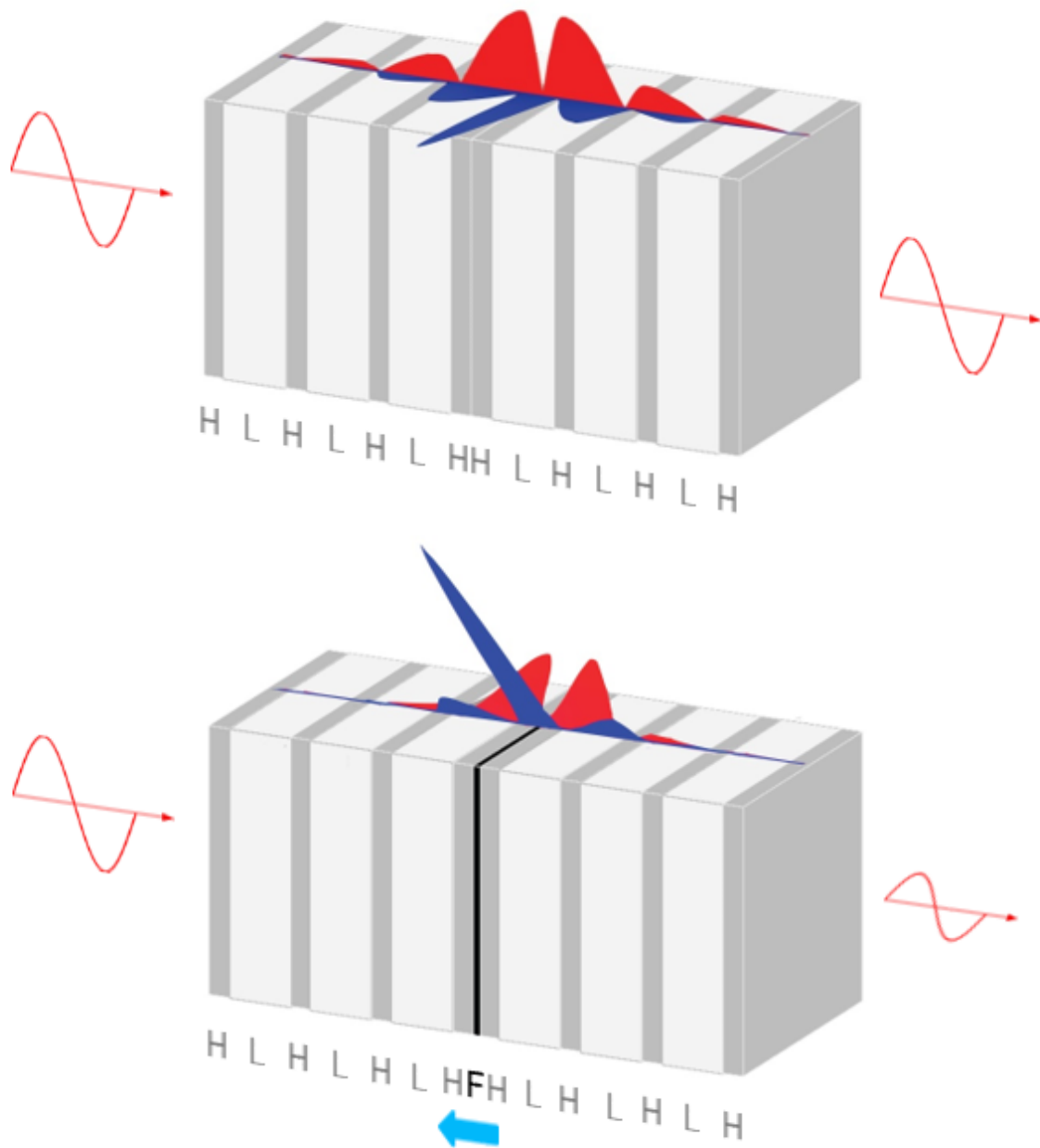
Figure 4.3 3C3 Photonic Structure with Faraday Rotation (Note: The "F" represents the Cobalt layer)

The MW permittivity of cobalt is large and almost purely imaginary.

$$\epsilon_C \approx \frac{4\pi\sigma_C}{\omega} i \tag{4.21}$$

where ω is the angular frequency, and the electric conductivity of cobalt is $\sigma_C = 1.44 \times 10^{-17} s^{-1}$ [21]. Stand-alone metallic layers are highly reflective to MW radiation even at thicknesses far less than the skin depth, due to multiple reflections in the metallic layer [59]. The MW transmittance of a cobalt layer of thickness d_C at frequencies not too close to the ferromagnetic resonance can be approximated by

$$T \approx \frac{1}{\left(1 + \frac{2\pi d_C \sigma_C}{c}\right)^2} \tag{4.22}$$

where c is the speed of light. For example, for $d_C = 33\ nm$, $T \approx 10^{-4}$.

The MW permeability of cobalt is described by the Polder permeability tensor [34] and a further description can be found in Section 4.1. We assume that a static uniform magnetic field is applied perpendicular to the cobalt layer along the wave propagation direction (z-axis in Figure 4.3) and that the internal static field, H_i, saturates the cobalt layer whose magnetization M_0 is oriented along the z-axis. In the presence of the MW electromagnetic field, h (where $h \ll H_i$), which is applied perpendicular to the z-axis, the ac component of the internal flux density, b, is given by $b = \hat{\mu}h$, where the permeability tensor μ is

$$\hat{\mu} = \begin{vmatrix} \mu & i\mu_a & 0 \\ -i\mu_a & \mu & 0 \\ 0 & 0 & 1 \end{vmatrix} \tag{4.12}$$

With the elements

61

$$\mu = 1 + 4\pi\chi = \frac{\omega_H(\omega_H + \omega_M) - \omega^2}{\omega_H^2 - \omega^2}, \qquad \mu_a = 4\pi\chi_a = \frac{\omega\omega_M}{\omega_H^2 - \omega^2} \qquad (4.13)$$

where $\omega_H = \gamma H_i$, $\omega_M = \gamma 4\pi M_0$, $\gamma/2\pi = 2.8\ GHz/kOe$ is the gyromagnetic ratio, and α is the dissipation parameter. Here we use the cobalt parameters [60], $4\pi M = 17900\ G$ and $\alpha = 0.027$.

The nonreciprocity of cobalt is determined via the off-diagonal elements of the permeability tensor. One can show that for circular polarized waves the permeability tensor becomes diagonal with the effective permeabilities.

$$\mu_\pm = 1 + 4\pi\chi_\pm = \mu \pm \mu_a = \frac{\omega_H + \omega_M \mp \omega}{\omega_H \mp \omega} \qquad (4.15)$$

Where the resonant behavior occurs only for the right (+) circularly polarized wave. For $\alpha \ll 1$, the imaginary part of μ_+, which is responsible for magnetic losses, is important only in the vicinity near the ferromagnetic resonance, $\omega_H^2 = (1 + \alpha^2)\omega^2$, where it develops a steep maximum [61] (See Figure 4.1). On the other hand, the real part of μ_a, $\mu_a' = \Re(\mu_a)$, which is responsible for magnetic circular birefringence. Remains considerable even far from resonance where it can be approximated as $\mu_a' \approx \omega_M\omega/(\omega_H^2 - \omega^2)$.

We consider a linearly polarized MW field normally incident on the magneto-photonic (MP) structures. Designating the incident, reflected and transmitted electric field components by E_i, E_ρ, and E_τ, respectively, we define the complex reflection and transmission coefficients of the MP structure, $\rho = |\rho| \exp(i\varphi)$ and $\tau = |\tau| \exp(i\phi)$, by $E_\rho = \rho E_i$ and $E_\tau = \tau E_i$. The reflectance R and transmittance T are given by $R = |\rho|^2$ and $T = |\tau|^2$, and the absorptance A is $A = 1 - R - T$. Since the linearly polarized incident wave can be considered as composed of two circularly polarized components of equal amplitude, the reflected and transmitted waves are

in general elliptically polarized due to the difference in the permeabilities μ_+ and μ_- of equation 5.4. For the transmitted wave, the Faraday rotation of the plane of polarization of the wave relative to the incident polarization is $\theta_{FR} = (\phi_+ - \phi_-)/2$, and the Faraday ellipticity is $e_F = (|\tau_+| - |\tau_-|)/(|\tau_+| + |\tau_-|)$ [62]. The transfer-matrix method (See Section 1.2) is used to calculate the variation of ρ and τ with wave frequency f, cobalt thickness d_C and internal magnetic field H_i.

4.3.3: Numerical Results

The frequency response of the $3C3$ structure in the vicinity of the transmission resonance as a function of detuning $\delta f = f - f_0$ is presented in Figure 4.4. The transmission of linearly polarized incident wave (solid blue line) can be decomposed into the sum of two components, $|\tau_+|^2$ and $|\tau_-|^2$, shown in Fig. 4.4(a) by dotted and broken lines, respectively. The splitting of the transmission resonance into two peaks is caused by the difference in the magnetic permeability for the left and right circularly polarized waves propagating in the direction of M_0. The amount of the splitting depends on the cobalt thickness d_C and the internal magnetic field H_i. It increases with increasing d_C and as H_i approaches the resonance field $2\pi f_0/\gamma$. In the vicinity of the resonance peak, the transmission phase (ϕ_+ and ϕ_-, shown in Figure 4.4(b) by the dotted and broken lines, respectively) increases by π, so that the Faraday rotation θ_{FR} (shown by a solid black line) has a maximum at $\delta f = 0$. Note that the pure Faraday rotation of a linearly polarized wave, i.e., with no wave ellipticity, occurs when $|\tau_+| = |\tau_-|$, and thus falls between the resonance peaks. The $3C3$ structure can be optimized for pure 45° Faraday rotation by adjusting the separation of the resonance peaks with a proper combination of d_C and H_i. A $\pi/2$-phase difference occurs at the midpoint between the two resonances at which $|\tau_+| = |\tau_-|$ when the resonance separation is equal the the FWHM of the resonance.
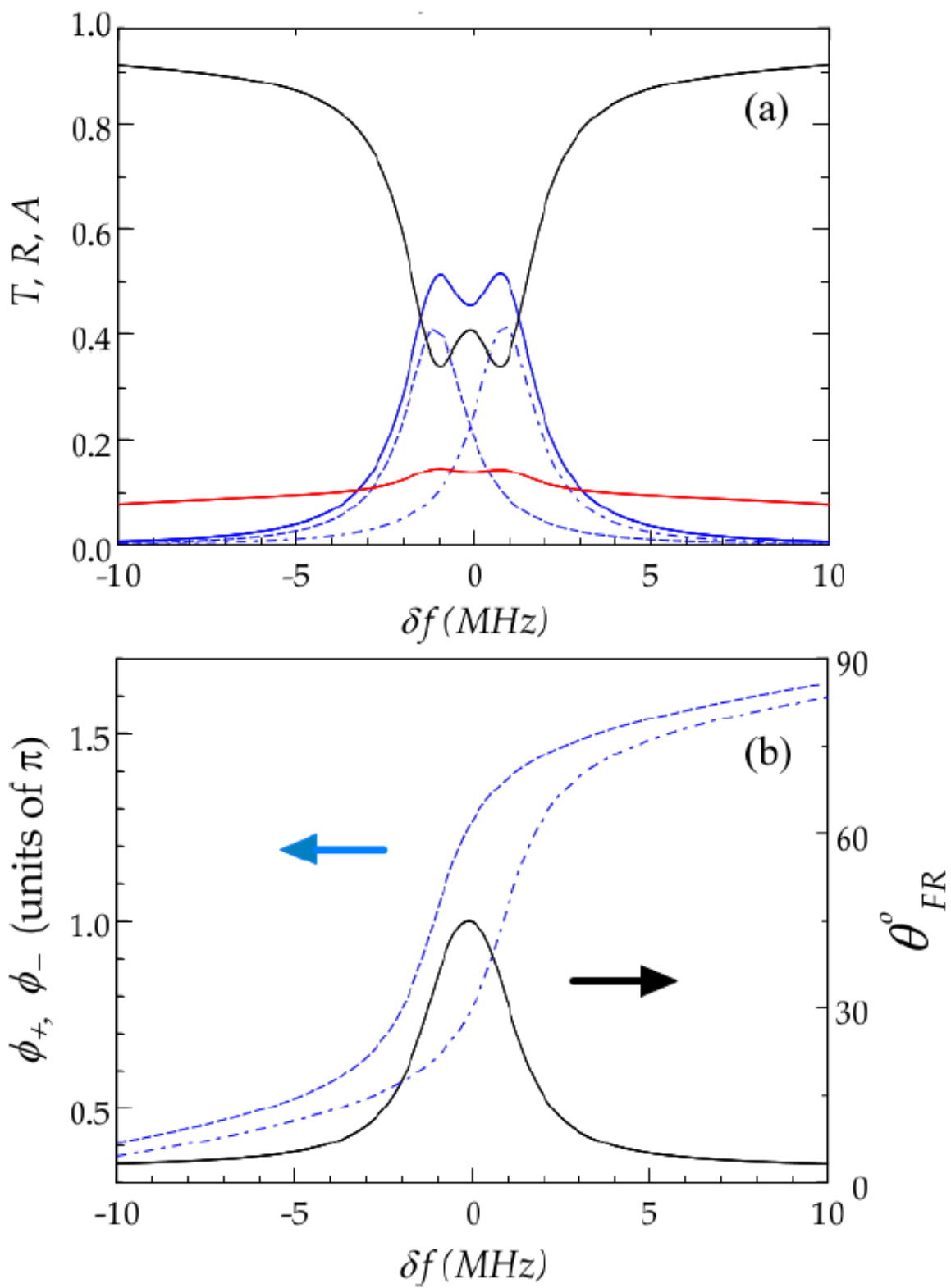
Figure 4.4 3C3 Frequency Response

In Figure. 4.5, the $3C3$ structure is optimized for a pure 45° Faraday rotation with $d_c = 180nm$ and $H_i = 0.1kOe$. The corresponding transmittance $T_{45°}$ is 0.46, which is only slightly below $T_{45°} = 0.5$ for the case of no absorption. The absorptance and reflectance are show in Figure 4.4(a). For NCN structures, there is a range of combinations of d_c and H_i for the pure 45° Faraday rotation. A few such combinations with corresponding values of $T_{45°}$ are shown in Fig 5.3 for $N = 2$ (circles), $N = 3$ (squares), and $N = 4$ (triangles). Except for $N = 2$, high values of $T_{45°}$ occur both above and below the resonant field, $2\pi f_0/\gamma = 2.68 \ kOe$, at which $T_{45°}$ vanishes due to magnetic circular dichroism. Note that in Fig. 5.3 suitable values of cobalt thickness d_c differ by orders of magnitude for different N, falling to tens of nanometers for $N = 4$

Figure 4.5 NCN photonic Structure optimized for 45-degree Faraday Rotation

4.3.4: Coupled Resonators

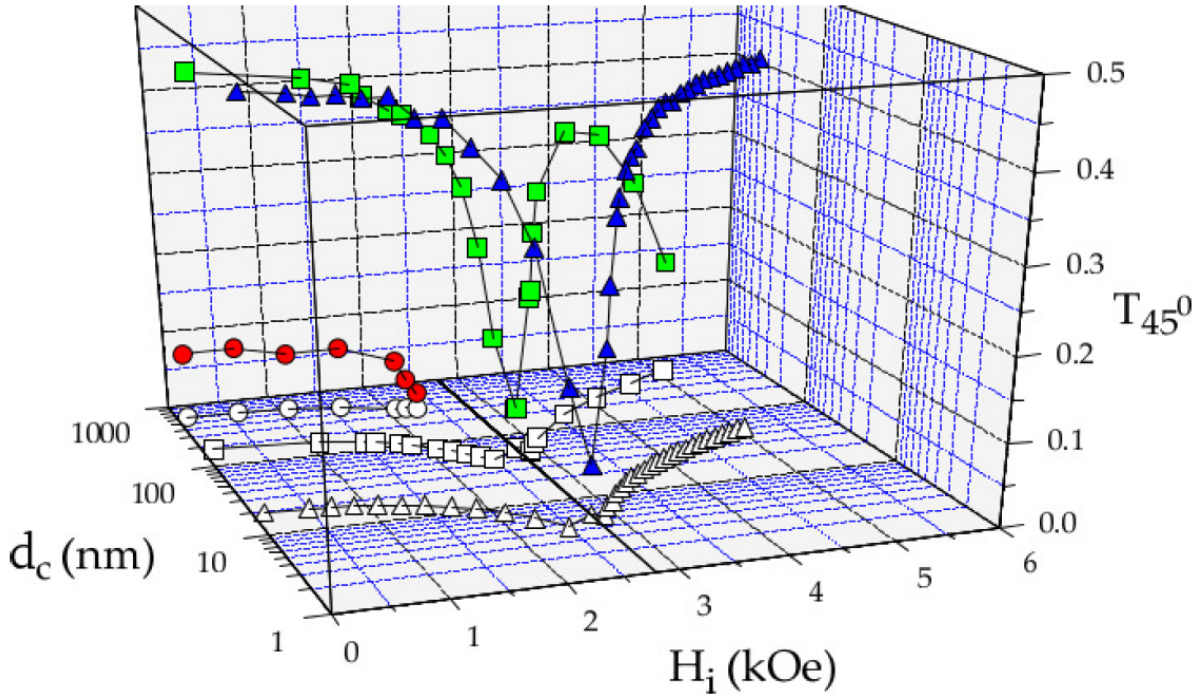The periodic arrangement with multiple defects, $N:M:N$, $N:M:M:N$, etc. can be considered as a superlattice of $N:N$ structures coupled via phase-matching air layers, or coupled-resonance structures (CRS) (cf. [63]). As a result of the coupling, the eigenmodes of the individual $N:N$ structures split into a miniband of polarization-degenerate localized states contered at the midgap frequency f_0 of the $N:N$ structure. The miniband width depends on the coupling strength, and thus on N. One of the most important properties of CRS is that the dispersion relation and the transmission spectrum for a moderate number of unit cells of the super-lattice can be optimized to close approximate that of the infinite CRS [64, 65]. As a result, the transmission phase via a finite-size CRS exhibits a smooth increase through a finite and high transmission mini-band summing up to a total phase shift equal to the number of half-wave defects in the structure multiplied by π [65]. When magnetic layers are introduced into the finite-size CRS, it is possible to achieve a uniform Faraday rotation in a finite and high transmission mini-band.

The frequency response of the $3C7C3$ structure (2-unit cell CRS) is presented in Figure 4.6. As in the $3C3$ structure, the cobalt layers lift the polarization degeneracy of localized modes, resulting in splitting of transmission resonance for $|\tau_+|^2$ and $|\tau_-|^2$ (Fig. 4.6a). In contrast to the $3C3$ structure, however, each of the two resonances represents a band of two overlapping localized modes. The transmission phases ϕ_+ and ϕ_- increase by 2π through the resonances (Fig. 4.6b), and the pure $45°$ Faraday rotation can be achieved with a smaller resonance separation (note the different scales on the frequency axes in Figs. 4.4 and 4.6). This, in turn, leads to a significantly higher transmittance, $T_{45°} = 0.82$, as compared to the $3C3$ structure. The results of $d_C = 70\ nm$ and $H_i = 0.1\ kOe$. We note that a wider and higher transmission mini-

band of the pure 45° Faraday rotation can be obtained with a larger number of unit cells of the

CRS.
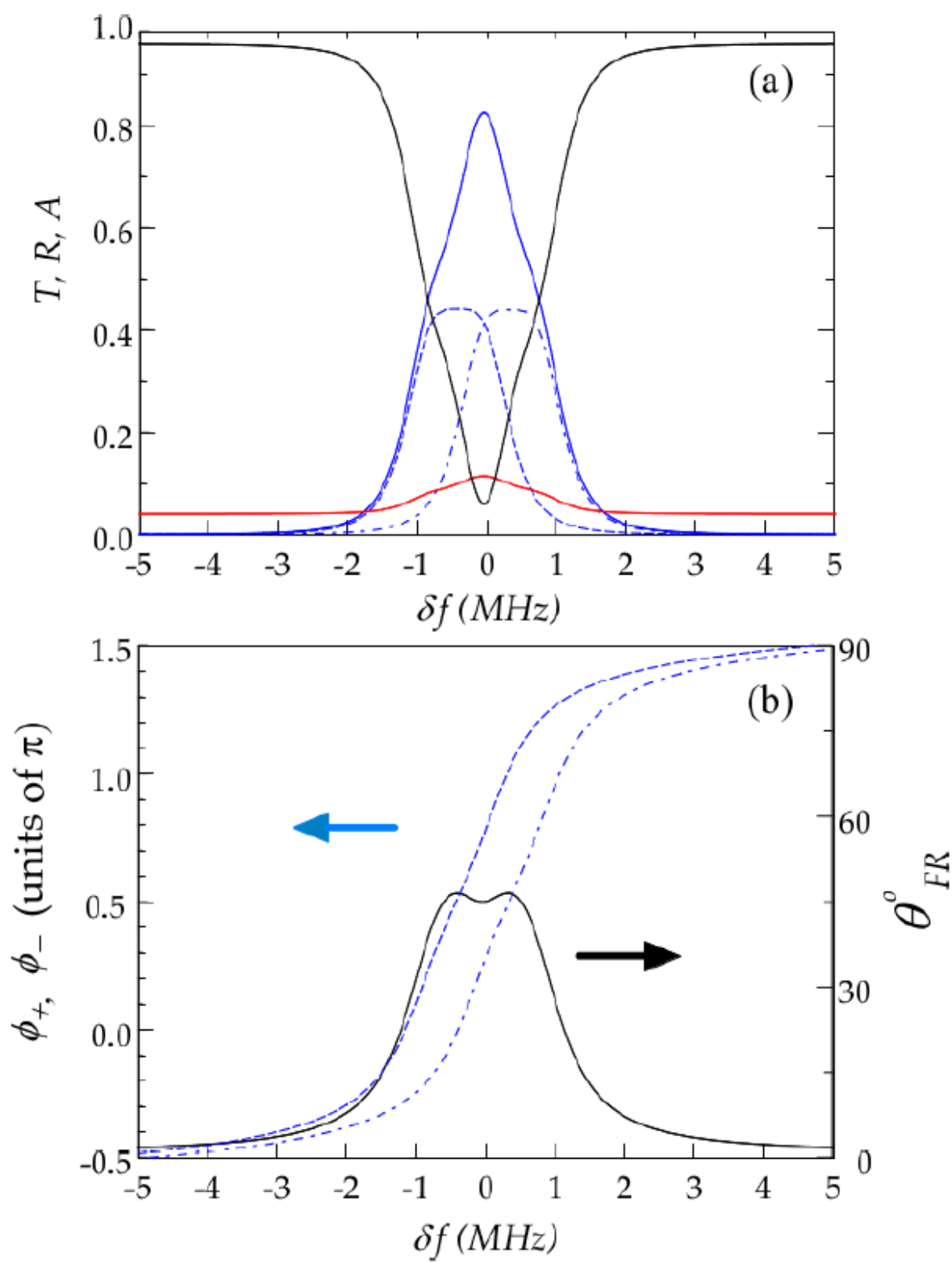
Figure 4.6 3C7C3 Structure

4.3.5: Microwave Isolation

When the magneto-photonic structure $3C3$ or $3C7C3$ are placed between linear polarizers with a 45° misalignment angle between their acceptance planes, the entire structure acts as a MW isolator (See Figure 4.7). For the forward (FW) transmission, the incident wave will rotate 45° and match the entering and exiting polarizers, providing high transmission. For the backward (BW) transmission, the nonreciprocal rotation of 45° in addition to the initial 45° from the polarizer will yield a 90° exiting wave, thus crossing the final polarizer, thus causing a dip in the backward transmission. The Faraday rotation induced by the $3C3$ is limited by a small ellipticity of the transmitted wave but still exhibits an isolation of over$-40\ dB$. The 3C3 structure is optimized for a 45° Faraday rotation with $d_C = 180\ nm$ and $H_i = 0.1\ kOe$.
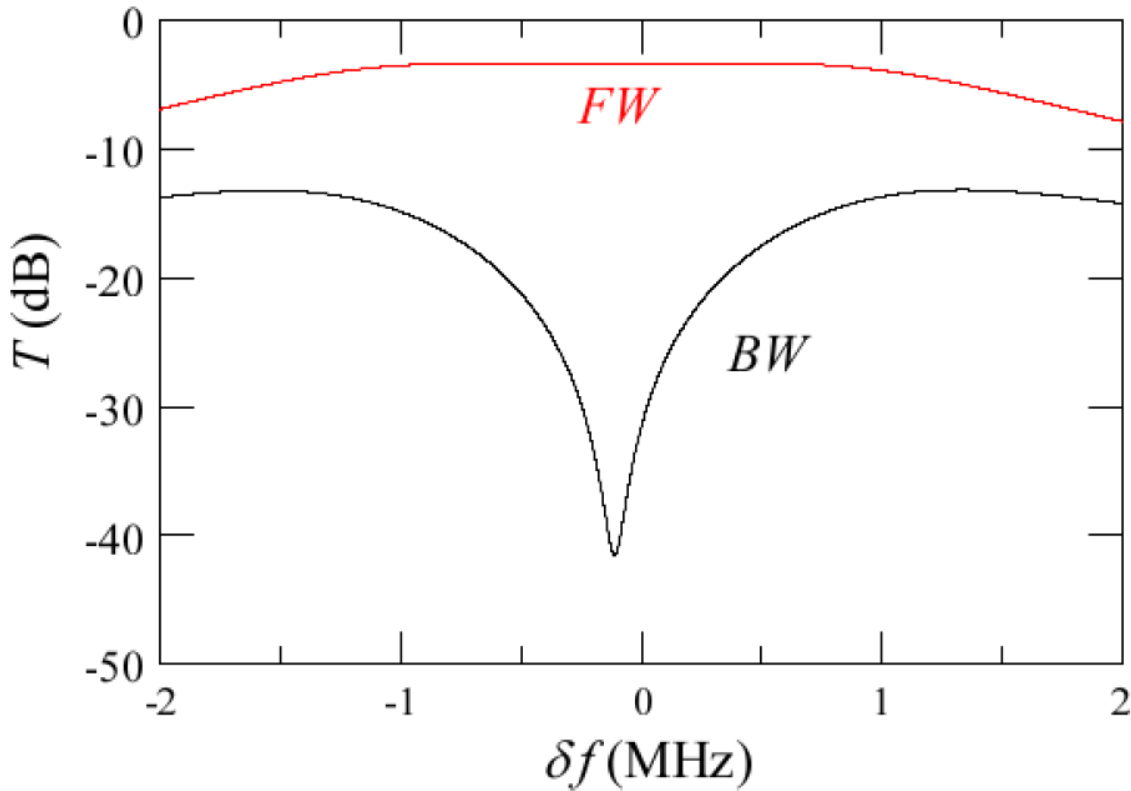
Figure 4.7 Isolation for 3C3 structure

In chapter 3, there was a brief discussion on how this same photonic structure can conditionally induce transmission for only one particular angle of incidence. This was done with the use of an asymmetrical defect that appears degenerate for some incident angle (See Section 3.2). With this added consideration, our magnetophotonic structure can provide more extreme directionality to the isolation. In such a case, the layered structure becomes extremely directional and only transmits the incident radiation r one angle (say normal incidence) and with a narrow frequency band. When such a structure is placed between linear polarizers like that described above, radiation will only pass along the $+z$ direction. We must emphasize that such an extreme directionality for the asymmetric layered structure is caused by high electric conductivity of the metallic layer (See Figure 3.1).

4.4: Conclusion

In this chapter, we discussed that the aforementioned metal-dielectric photonic structure can be elevated to a magneto-photonic structure when the metal is a ferromagnetic metal. This structure is capable of high transmission and enhanced nonreciprocal response – namely to provide 45° Faraday rotation. Such a structure can be realized as a omni-directional microwave isolator. Additionally, such a resonator can be strung together in succession with other resonators to create a super lattice capable of generating mini-bands of transmission and 45° Faraday rotation. When the location of the metallic layers inside the resonant cavities coincides with the electric field node, conductivity losses are suppressed by four to six orders of magnitude. Additionally, the magnetic Faraday rotation is enhanced because the ferromagnetic layers are located at the antinodes of the oscillating magnetic field. As a result, the layered structure becomes nearly perfectly transmissive, while producing a strong, 45° Faraday rotation. By contrast, depending on its thickness, a stand-alone ferromagnetic metallic layer would be either totally reflective, or would not produce any measurable Faraday effect at all. In addition, a combination of high electric conductivity and magnetic circular birefringence of the metallic magnetic layers can lead to extreme transmission directionality of the layered structure.

CHAPTER 5: OBLIQUE INCIDENCE

5.1: Results

Let us now discuss the case of oblique incidence. The transmission spectrum for a similar structure to that in Chapter 2 is presented in Figure 5.1. At oblique incidence, the effect of induced transparency does not go away, but the respective resonance frequency increases with the incident angle, as shown in Figure 5.1(a). Qualitatively, this behavior is the same for both TE and TM polarizations.

At the resonant frequency, the position of the metallic layer must coincide with the node of the electric field to induce transmission. In all cases involving the symmetric structure of Figure 2.1, the resonance conditions automatically imply that the introduced metallic layer is indeed located at the electric field node. If we modify the defect by making it asymmetric, the induced transparency vanishes for all frequencies and all incident directions. We can modify the defect layers, however, so that the induced transparency only persists at normal incidence, as shown in Fig. 5.1(b). In such a case, the layered structure becomes extremely directional and only transits the incident radiation at normal incidence and with a narrow frequency band. We emphasize that such an extreme directionality of the asymmetric layered structure is caused by high electric conductivity of the metallic layer. Indeed, when the metallic layer is replaced by a non-conducting magnetic material of the (see Figure 5.1(c)), the effect of extreme directionality of Figure 5.1(c) goes away.
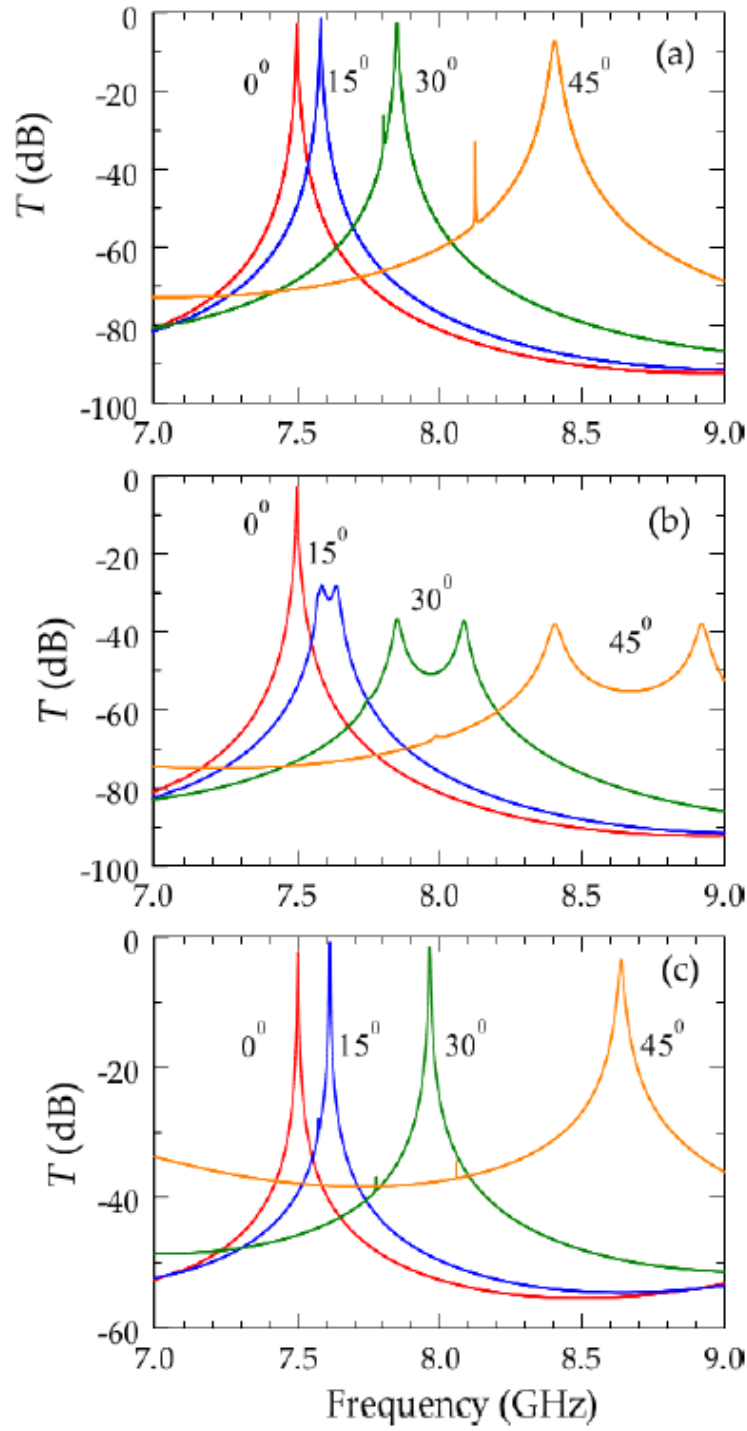
Figure 5.1 Transmission spectra for 3C3 structure with symmetric (a) and asymmetric (b) defect at oblique incidence. In the latter case, as the angle of incidence increases, the transmission spectra are increasingly blue shifted and strongly reduced due to reflection from the metallic layer as compared to that of normal incidence. (c), when the cobalt layer is replaced by a non-conductive magnetic layer of the same thickness, the magneto-photonic structure remains transmissive.

5.2: Conclusion

We have seen that a properly designed photonic layered structure incorporating the same metallic magnetic layer (Cobalt) becomes totally transmissive and, at the same time, produces strong Faraday rotation. Moreover, the nonreciprocal metal-dielectric structure can display extreme directionality, transmitting the incident radiation only in a single (forward) direction, while blocking radiation incident from all other directions. This unique feature is due to strong electric conductivity of the metallic layer. One immediate application is a wide-aperture omnidirectional isolation. Similar nonreciprocal metal-dielectric photonic structures can be designed for THz and far infrared frequencies.

CHAPTER 6: MICROWAVE MEASUREMENTS OF FARADAY ROTATION IN MAGNETIC METAL-DIELECTRIC PHOTONIC STRUCTURES

6.1: Introduction

In Chapter 2, we described experimental results regarding the induced transparency of a ferromagnetic metal inside our photonic structure design (See Section 2.4). We will resume this discussion now with further consideration to the magnetic nature of the photonic structure. Namely, we will showcase through experiment that the magneto-photonic structure described in the section 2.4 is capable of providing induced transmission and 45° Faraday rotation for a given applied magnetic field. Experiments were done at the National High Magnetic Field Lab (NHMFL) in Tallahassee, Florida. For a full description of the setup, see Section 2.4.

6.2: Experimental Setup

We will recall the experimental structure. The photonic structure was a defect photonic crystal of the same essential design as that in our numerical setup. The unit cell consists of a two dielectric layers, a high index ceramic layer ($\epsilon_A = 38.09 + 0.0095i$, $d_A = 1.046\ mm$) and a low index glass layer ($\epsilon_B = 3.75$, $d_B = 3\ mm$). These layers were arranged to create the $3:3$ structure. Then, at the center of the half-wave defect, a CoFe nanolayer ($d_C = 150\ nm$) was added. The CoFe was deposited on a $525\ \mu m$ glass substrate. To ensure that our 3C3 structure is symmetrical, a blank glass substrate was added to the film side of the CoFe layer to create symmetric defect.

6.3: Numerical Results

In Figure 6.1, we show the evolution of the frequency response for various applied magnetic field. Here we see that only one transmission polarization is affected by the magnetic field. To better understand this, we can recall the expression for the magnetic permeability for a ferromagnet magnetized to saturation:

$$\mu_\pm = 1 + 4\pi\chi_\pm = \mu \pm \mu_a = \frac{\omega_H + \omega_M \mp \omega}{\omega_H \mp \omega} \tag{4.15}$$

Here we see that when the ferromagnetic resonance condition is met, a singularity appears and based on the discussion in section 4.1, one component will become completely absorbed (such is called circular dichroism). This can be seen in the top panel of Figure 6.1 for the T_+ component. As the magnetic field sweeps closer to the ferromagnetic resonance (when the horizontal axis is equal to unity), the resonance shifts away from the reference frequency (where the vertical axis is zero) and decreases in transmission. For the T_- component (lower panel of Figure 6.1), we see a negligible change to the transmission spectrum with applied magnetic field.
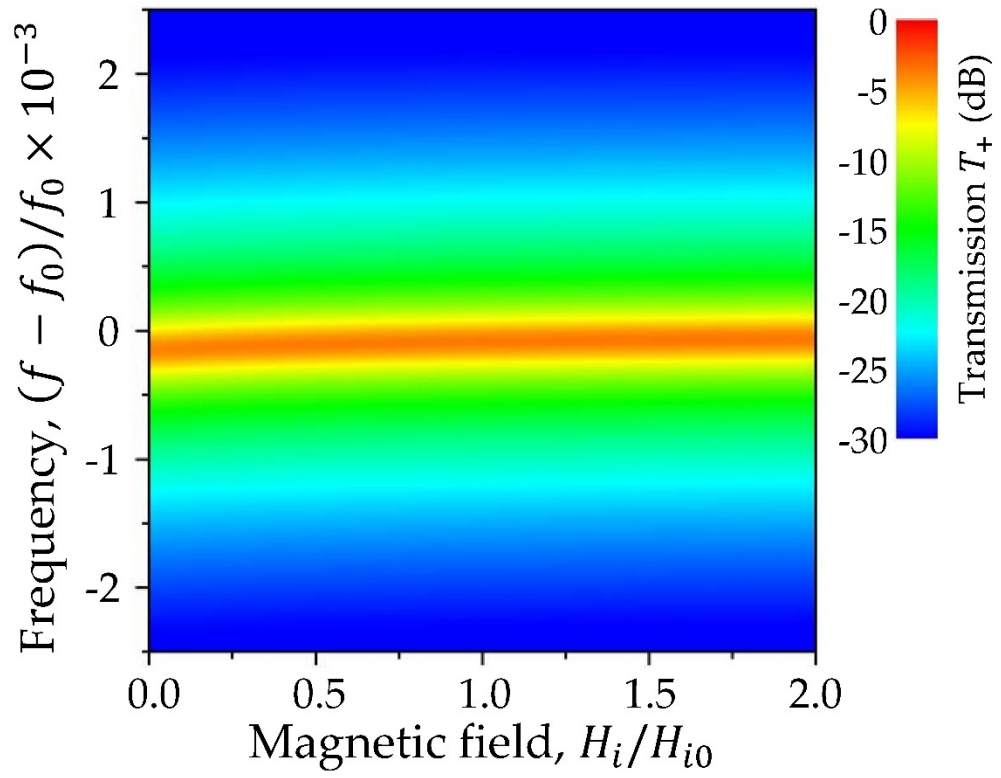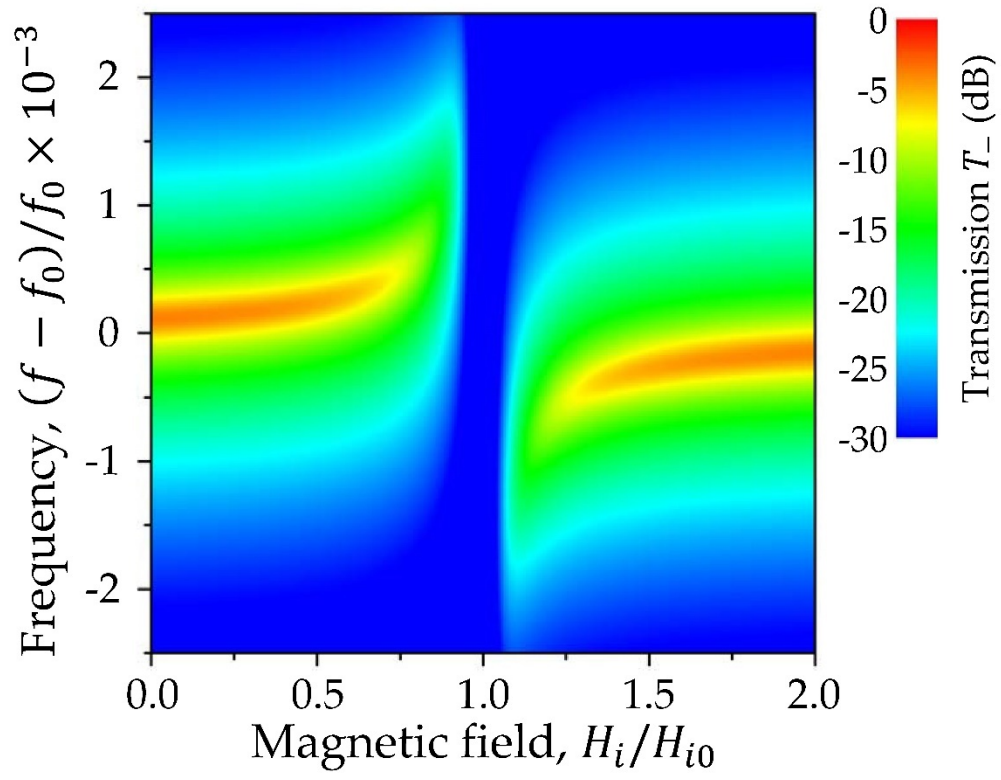
Figure 6.1 Experimental Structure Color-plot

A numerical simulation of the frequency response of the experimental structure is provided in Figure 6.2. By comparison, these results are qualitatively the same as Figure 4.4. Again, we show the frequency response with a horizontal axis that has been scaled and normalized as a detuning from the reference frequency f_0; where the reference frequency is represented on this axis as zero. The total transmission of a linearly polarized incident wave (solid red line, Figure 6.2, upper panel) can be decomposed into the sum of two components, T_+ and T_-, shown in the upper panel of Figure 6.2 by solid and broken black lines, respectively. In Figure 6.2, the applied magnetic field is $H_{ext} = 21.6 \; kOe$, and is in the vicinity of the ferromagnetic resonance (ω is near ω_H). Because of this, there is a lifted degeneracy between left and right circular polarizations, and splitting between the respective transmission resonances occurs (See Figure 6.2, top panel). It is at this particular applied magnetic field that we achieve 45° Faraday rotation (green) with negligible ellipticity (purple) near the reference frequency (See Figure 6.2, lower panel). Much like the numerical simulations show in in the earlier section, the magneto-photonic structure will provide high transmission ($T \approx 0.5$) and 45° pure Faraday rotation.
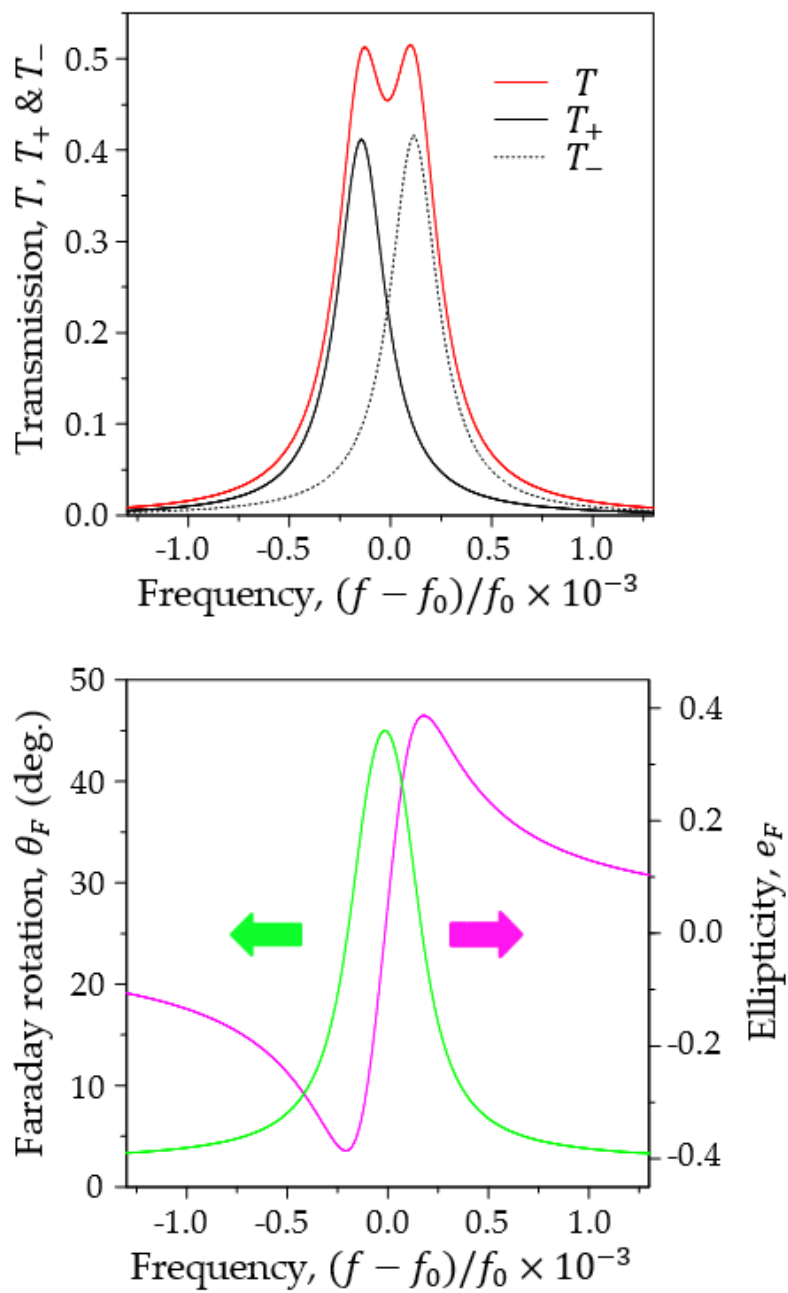
Figure 6.1 3C3 with CoFe

6.4: Experimental Results

With a closer look at Figure 6.2, we see that the maximum of Faraday rotation coincides with a point of zero ellipticity (or when $|T_+| = |T_-|$). Where there is no ellipticity, we have pure Faraday rotation which is ideal for isolators. In Figure 4.10, we show the transmission and Faraday rotation as a function of applied external magnetic field when this condition is met. In other words, the value of transmission and Faraday rotation when the ellipticity is zero. This point usually resides at a frequency between the two circular polarized peaks (e.g., at zero in Figure 6.2).

In Figure 6.3, we see in the top panel that there is a drop in transmission at the ferromagnetic resonance condition (at $H_{FMR} = 21.4\ kOe$, marked by a dotted vertical line in both plots). This point corresponds to circular dichroism where one circular polarization is completely absorbed. When the applied magnetic field is just above or below this condition, the magnetic absorption is not at a maximum (See Figure 4.1), thus there is only a nonreciprocal differential phase shift between the two circularly polarized transmission; this allows for a circular birefringence is occur and thus Faraday rotation to become large. We see two extrema of faraday rotation on either side of the ferromagnetic resonance (See lower panel of Figure 6.3). Each of these extrema reach higher than 45° pure Faraday rotation with still a sizable transmission (Note: the top panel displays just one circular polarizations transmission).
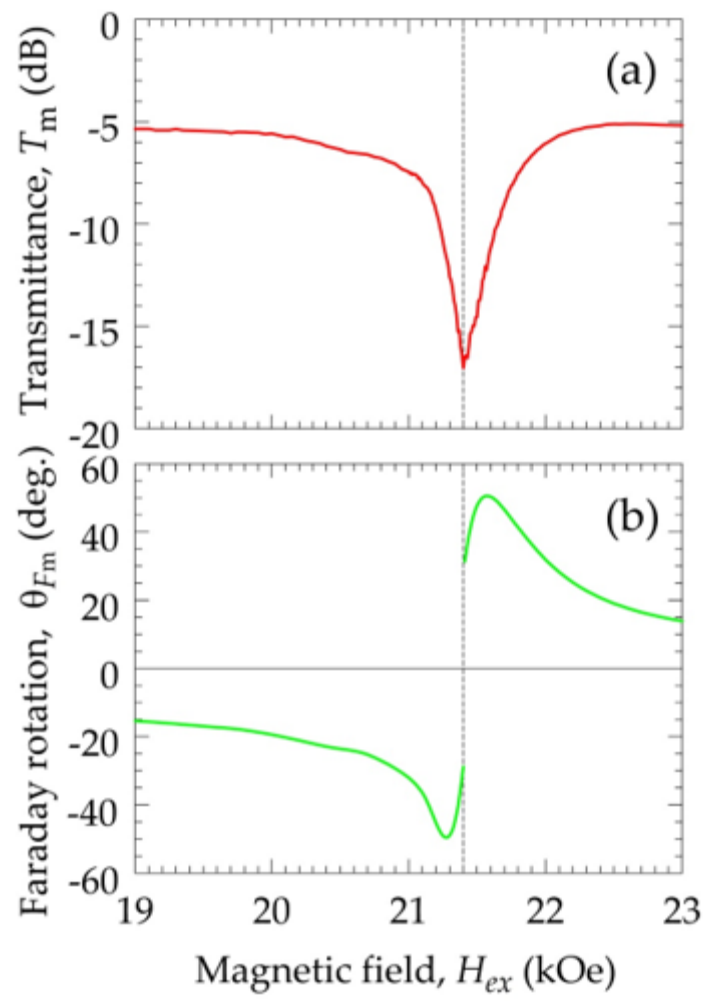
Figure 6.2 Transmission and Faraday Rotation with zero Ellipticity

6.5: Conclusion

Based on experiments at the NHMFL, we are able to build a magneto-photonic structure capable of induced transmission and 45° Faraday rotation. By placing the ferromagnetic metal layer at the node of electric field in the photonic structure, conductivity losses can be dramatically suppressed allowing for high transmission. Additionally, because the ferromagnet is placed where the oscillating magnetic field is an antinode, there is a large nonreciprocal response, i.e. circular birefringence, which can be controlled by the applied magnetic field.

CHAPTER 7: DISSERTATION CONCLUSION

In summary, we have demonstrated that a properly designed magnetic metal–dielectric photonic structure can not only become highly transmissive at microwave frequencies, but it can also produce a large Faraday rotation. Remarkably, the same metallic ferromagnetic layer taken out of the layered structure is neither transmissive, nor does it produce any measurable Faraday rotation. Strong Faraday rotation in combination with a high transmission is achieved by placing ferromagnetic metallic nanolayer in a node of the electric field component of the quasi-localized electromagnetic mode of the layered structure, which results in simultaneous reduction of the Ohmic losses (by up to 5 orders of magnitude) and enhancement of the magnetic Faraday rotation (by up to 2 orders of magnitude). This approach can be utilized for any lossy magnetic material of considerable magnetic gyrotropy, provided that the gyrotropy is predominantly associated with the permeability tensor, while the losses are caused by the electric conductivity. Such magnetic materials are readily available at MW frequencies. Some examples can also be found at higher frequencies, including far infrared. Using the example of ferromagnetic cobalt, we demonstrated that a 45-degree Faraday rotation and high transmission in a finite frequency band can be obtained with metallic layers as thin as a hundred of nanometers. These results suggest that photonic structures involving conducting ferro- or ferrimagnetic components can be used in various nonreciprocal photonic devices from MWs to far infrared.

We have also introduced a photonic layered structure design with hypersensitive transport characteristics. This layered structure consists of an asymmetric dielectric cavity incorporating a metallic nanolayer and sandwiched between two Bragg mirrors. When the metallic nanolayer coincides with the nodal point of the localized mode, the system develops the phenomenon of induced transmission. However, even a small change in the refractive index of

85

one of the dielectric layers of the asymmetric cavity abruptly suppresses the localized mode and renders the layered structure highly reflective at all frequencies – not just at frequencies of the photonic band gap. Thus, these metal-dielectric structures can be used as hypersensitive microwave and optical limiters. Specifically, at low incident wave intensity, these structures support a narrow-band transmission. If the electromagnetic wave intensity exceeds certain level, even a small self-induced change (due to nonlinearities or heating effects) in the refractive index of the asymmetric layer causes an abrupt transition to a broadband reflectivity. The proposed design can be adjusted to different frequency ranges starting from microwave frequencies and up to the mid infrared. The concept of hypersensitive layered structures can be applied not only to electromagnetic waves but also to acoustic waves, matter-waves, etc.

AUTHOR BIBLIOGRAPHY

- Smith, K. and A. Chabanov (2011). "Enhanced Transmission and Nonreciprocal Properties of a Ferromagnetic Metal Layer in One-Dimensional Photonic Crystals." Integrated Ferroelectrics 131(1): 66-71.

- Smith, K., et al. (2012). "Enhanced Transmission and Giant Faraday Effect in Magnetic Metal-Dielectric Photonic Structures." arXiv preprint arXiv:1212.4393.

- Smith, K., et al. (2013). "Enhanced transmission and giant Faraday Effect in magnetic metal-dielectric photonic structures." J. Phys. D: Appl. Phys 46: 165002.

- Carroll, T. K., I. Vitebskiy, K. Smith, and A. A. Chabanov. "A concept of wide-aperture omnidirectional isolation based on metal-dielectric magneto-photonic structures." In Avionics, Fiber-Optics and Photonics Technology Conference (AVFOP), 2014 IEEE, pp. 59-60. IEEE, 2014.

- Makri, Eleana, Kyle Smith, Andrey Chabanov, Ilya Vitebskiy, and Tsampikos Kottos. "Hypersensitive Transport in Photonic Crystals with Accidental Spatial Degeneracies." Scientific reports 6 (2016).

AUTHOR PRESENTATIONS

1. K. Smith and A. A. Chabanov, Enhanced electromagnetic wave transmission and Faraday rotation of a ferromagnetic metal layer embedded in dielectric slab 5th International Congress on Advanced Electromagnetic Materials in Microwaves and Optics – Metamaterials 2011 Barcelona, Spain, 10-15 October 2011

1. K. Smith, T. Carroll, J.D. Bodyfelt, I. Vitebskiy, and A. A. Chabanov, Nonreciprocal metal-dielectric photonic structures with extreme directionality, 7th International Congress on Advanced Electromagnetic Materials in Microwaves and Optics – Metamaterials 2013 Bordeaux, France, 16-21 September 2013

2. A. Chabanov, K. Smith, T. Carroll, and I. Vitebskiy, Nonreciprocal Metal-Dielectric Photonic Structures with Extreme Directionality: A Concept of Wide-Aperture Omnidirectional Isolator, 8th International Congress on Advanced Electromagnetic Materials in Microwaves and Optics – Metamaterials 2014 Copenhagen, Denmark, 25-30 August 2014

3. E. Makri, K. Smith, A. Chabanov, I. Vitebskiy, and T. Kottos, Hypersensitive Transport in Asymmetric Photonic Layered Media, 10th International Congress on Advanced Electromagnetic Materials in Microwaves and Optics - Metamaterials 2016 Crete, Greece, 17-22 September 2016

4. K. Smith and A. A. Chabanov, Microwave Faraday Effect in 1D Cobalt Magnetophotonic Crystals, Conference on Lasers and Electro-Optics - CLEO 2012 San Jose, California, USA, 6-11 May 2012

5. K. Smith, T. Carroll, J.D. Bodyfelt, I. Vitebskiy, and A. A. Chabanov, Nonreciprocal metal-dielectric photonic structures with extreme directionality, Conference on Lasers and Electro-Optics - CLEO 2013 San Jose, California, USA, 8-13 June 2013

6. K. Smith, T. Carroll, J.D. Bodyfelt, I. Vitebskiy, and A. A. Chabanov, Nonreciprocal photonic structures with extreme directionality, Donostia International Conference on Nanoscaled Magnetism and Applications - DICNMA 2013 San Sebastian, Spain, 1-4 September 2013

7. K. Smith and A. A. Chabanov, Microwave Faraday Effect in Magnetophotonic Crystals, Electrical transport and optical properties of inhomogeneous materials - ETOPIM 2012 Marseille, France, 2-7 September 2012

8. K. Smith and A. A. Chabanov Enhanced Microwave Transmission and Faraday Effect in Magnetophotonic Crystals Progress in Electromagnetics Research Simposium - PIERS 2012 Moscow, Russia, 19-23 August 2012

9. Kononchuk R., Smith K., Chabanov A.A., Makri E., Kottos T., and Vitebskiy I. Hypersensitive Transport in Asymmetric Photonic Layered Media Days on Diffraction, International Conference St Petersburg, Russia, 27 June - 1 July 2016

10. Trevino C., Kononchuk R., Smith K., Vitebskiy I., and Chabanov A.A. Induced transmission and enhanced Faraday rotation in ferromagnetic thin fi lms Days on Diffraction, International Conference St Petersburg, Russia, 27 June - 1 July 2016

11. K. Smith, T. Carroll, I. Vitebskiy, and A. A. Chabanov, Nonreciprocal metal-dielectric photonic structures with extreme directionality, International Symposium on Multifunctionality of Ferroics and Multiferroics - INAMM 2014 San Antonio, TX, 10-11 October, 2014

APPENDIX A: THE REDUCED MAXWELL OPERATOR

The Reduced Maxwell Operator is a 4 x 4 matrix that appears when combining

Maxwell's equations together to build a system of four linear ordinary differential equations.

Each equation deals only with the tangential components (x and y components) of the electric

and magnetic fields which vary only with the z direction.

$$\partial_z \Psi(z) = i\frac{\omega}{c} M(z)\Psi(z) \qquad (A.1)$$

Where

$$\Psi(z) = \begin{bmatrix} E_x(z) \\ E_y(z) \\ H_x(z) \\ H_y(z) \end{bmatrix} \qquad (A.2)$$

To show this, we will start with the familiar Maxwell's equations

$$\nabla\times\vec{E}(\vec{r}) = i\mu(z)\frac{\omega}{c}\vec{H}(\vec{r}), \qquad \nabla\times\vec{H}(\vec{r}) = -i\epsilon(z)\frac{\omega}{c}\vec{E}(\vec{r}) \qquad (A.3)$$

Where we will assume the following:

$$\hat{\epsilon}(z) = \begin{bmatrix} \epsilon_{xx} & \epsilon_{xy} & \epsilon_{xz} \\ \epsilon_{yx} & \epsilon_{yy} & \epsilon_{yz} \\ \epsilon_{zx} & \epsilon_{zy} & \epsilon_{zz} \end{bmatrix}, \qquad \hat{\mu}(z) = \begin{bmatrix} \mu_{xx} & \mu_{xy} & \mu_{xz} \\ \mu_{yx} & \mu_{yy} & \mu_{yz} \\ \mu_{zx} & \mu_{zy} & \mu_{zz} \end{bmatrix} \qquad (A.4)$$

And

$$\vec{E}(\vec{r}) = e^{i(k_x x + k_y y)}\vec{E}(z), \qquad \vec{H}(\vec{r}) = e^{i(k_x x + k_y y)}\vec{H}(z) \qquad (A.5)$$

In equation A.4, we have kept the description of the permittivity and permeability general (for

now). In equation A.5, we are expressing that in which ever medium we are in, the fields will

only vary in phase along the tangential components. This in some sense is the description of any

stratified media. Considering now the curl of each field in Cartesian coordinates and Equation A.5:

$$\nabla\times\vec{E} = \left(ik_yE_z - \partial_zE_y\right)\hat{\imath} - \left(ik_xE_z - \partial_zE_x\right)\hat{\jmath} + \left(ik_xE_y - ik_yE_x\right)\hat{k}$$

$$\nabla\times\vec{H} = \left(ik_yH_z - \partial_zH_y\right)\hat{\imath} - \left(ik_xH_z - \partial_zH_x\right)\hat{\jmath} + \left(ik_xH_y - ik_yH_x\right)\hat{k}$$

$$(A.6)$$

This completes the left hand side of Equation A.3. Now for the right hand side,

$$-i\frac{\omega}{c}\hat{\epsilon}\vec{E} = -i\frac{\omega}{c}\begin{bmatrix}\epsilon_{xx} & \epsilon_{xy} & \epsilon_{xz}\\ \epsilon_{yx} & \epsilon_{yy} & \epsilon_{yz}\\ \epsilon_{zx} & \epsilon_{zy} & \epsilon_{zz}\end{bmatrix}\begin{bmatrix}E_x\\ E_y\\ E_z\end{bmatrix} = -i\frac{\omega}{c}\begin{bmatrix}\epsilon_{xx}E_x + \epsilon_{xy}E_y + \epsilon_{xz}E_z\\ \epsilon_{yx}E_x + \epsilon_{yy}E_y + \epsilon_{yz}E_z\\ \epsilon_{zx}E_x + \epsilon_{zy}E_y + \epsilon_{zz}E_z\end{bmatrix}$$

$$i\frac{\omega}{c}\hat{\mu}\vec{H} = i\frac{\omega}{c}\begin{bmatrix}\mu_{xx} & \mu_{xy} & \mu_{xz}\\ \mu_{yx} & \mu_{yy} & \mu_{yz}\\ \mu_{zx} & \mu_{zy} & \mu_{zz}\end{bmatrix}\begin{bmatrix}H_x\\ H_y\\ H_z\end{bmatrix} = i\frac{\omega}{c}\begin{bmatrix}\mu_{xx}H_x + \mu_{xy}H_y + \mu_{xz}H_z\\ \mu_{yx}H_x + \mu_{yy}H_y + \mu_{yz}H_z\\ \mu_{zx}H_x + \mu_{zy}H_y + \mu_{zz}H_z\end{bmatrix}$$

$$(A.7)$$

Substituting Equations A.6 and A.7 into A.3, and looking only to the last component of each, we can write a description of the normal components of the electric and magnetic fields.

$$ik_xE_y - ik_yE_x = i\frac{\omega}{c}\left(\mu_{zx}H_x + \mu_{zy}H_y + \mu_{zz}H_z\right)$$

$$\rightarrow \boxed{H_z = \mu_{zz}^{-1}\left(n_xE_y - n_yE_x - \mu_{zx}H_x - \mu_{zy}H_y\right)}$$

$$ik_xH_y - ik_yH_x = -i\frac{\omega}{c}\left(\epsilon_{zx}E_x + \epsilon_{zy}E_y + \epsilon_{zz}E_z\right)$$

$$\rightarrow \boxed{E_z = \epsilon_{zz}^{-1}\left(-n_xH_y + n_yH_x - \epsilon_{zx}E_x - \epsilon_{zy}E_y\right)}$$

$$(A.8)$$

Where $n_i = ck_i/\omega$. Now that we have a description of the normal components, we can look at the remaining tangential components and manipulate

$$\partial_z \begin{bmatrix} E_x \\ E_y \\ H_x \\ H_y \end{bmatrix} = i\frac{\omega}{c} \begin{bmatrix} -\mu_{yx}H_x - \mu_{yy}H_y - \mu_{yz}H_z - n_xE_z \\ \mu_{xx}H_x + \mu_{xy}H_y + \mu_{xz}H_z - n_yE_z \\ \epsilon_{yx}E_x + \epsilon_{yy}E_y + \epsilon_{yz}E_z - n_xH_z \\ -\epsilon_{xx}E_x - \epsilon_{xy}E_y - \epsilon_{xz}E_z - n_yH_z \end{bmatrix} \tag{A.9}$$

With our expressions for the normal components, E_z and H_z, from Equation A.8, we can expand the right hand side of Equation A.9 and collect terms such that the right hand side becomes $i\frac{\omega}{c}M\Psi$. The final result of which is

$$M(z) = \begin{bmatrix} M_{11} & M_{12} \\ M_{21} & M_{22} \end{bmatrix} \tag{A.10}$$

Where

$$M_{11} = \begin{bmatrix} -\dfrac{\epsilon_{zx}}{\epsilon_{zz}}n_x - \dfrac{\mu_{yz}}{\mu_{zz}}n_y & \left(-\dfrac{\epsilon_{zy}}{\epsilon_{zz}} + \dfrac{\mu_{yz}}{\mu_{zz}}\right)n_x \\ -\left(\dfrac{\epsilon_{zx}}{\epsilon_{zz}} - \dfrac{\mu_{xz}}{\mu_{zz}}\right)n_y & -\dfrac{\epsilon_{zy}}{\epsilon_{zz}}n_y - \dfrac{\mu_{xz}}{\mu_{zz}}n_x \end{bmatrix}$$

$$M_{12} = \begin{bmatrix} \mu_{yx} - \dfrac{\mu_{zx}\mu_{yz}}{\mu_{zz}} + \dfrac{n_yn_x}{\epsilon_{zz}} & \mu_{yy} - \dfrac{\mu_{zy}\mu_{yz}}{\mu_{zz}} - \dfrac{n_x^2}{\epsilon_{zz}} \\ -\mu_{xx} + \dfrac{\mu_{zx}\mu_{xz}}{\mu_{zz}} + \dfrac{n_y^2}{\epsilon_{zz}} & -\mu_{xy} + \dfrac{\mu_{zy}\mu_{xz}}{\mu_{zz}} - \dfrac{n_xn_y}{\epsilon_{zz}} \end{bmatrix}$$

$$M_{21} = \begin{bmatrix} -\epsilon_{yx} + \dfrac{\epsilon_{zx}\epsilon_{yz}}{\epsilon_{zz}} - \dfrac{n_yn_x}{\mu_{zz}} & -\epsilon_{yy} + \dfrac{\epsilon_{zy}\epsilon_{yz}}{\epsilon_{zz}} + \dfrac{n_x^2}{\mu_{zz}} \\ \epsilon_{xx} - \dfrac{\epsilon_{zx}\epsilon_{xz}}{\epsilon_{zz}} - \dfrac{n_y^2}{\mu_{zz}} & \epsilon_{xy} - \dfrac{\epsilon_{zy}\epsilon_{xz}}{\epsilon_{zz}} + \dfrac{n_xn_y}{\mu_{zz}} \end{bmatrix}$$

$$M_{22} = \begin{bmatrix} -\dfrac{\epsilon_{yz}}{\epsilon_{zz}}n_y - \dfrac{\mu_{zx}}{\mu_{zz}}n_x & n_x\left(\dfrac{\epsilon_{yz}}{\epsilon_{zz}} - \dfrac{\mu_{zy}}{\mu_{zz}}\right) \\ n_y\left(\dfrac{\epsilon_{xz}}{\epsilon_{zz}} - \dfrac{\mu_{zx}}{\mu_{zz}}\right) & -\dfrac{\epsilon_{xz}}{\epsilon_{zz}}n_x - \dfrac{\mu_{zy}}{\mu_{zz}}n_y \end{bmatrix} \tag{A.11}$$

APPENDIX B: DETERMINATION OF TRANSMISSION AND REFLECTION OF A STACK

The transfer matrix method allows one to determine a transfer matrix associated with a stack. It is this transfer matrix that can then be used to determine the evolution of the wave vector from one location to another. We will illustrate here the steps to determine the transmission and reflection coefficients, and thus the transmission and reflection.

Consider Equation 1.9,

$$\Psi^T = T\Psi_0 = T(\Psi_0^I + \Psi_0^R),$$

$$\Psi_0^I = \begin{bmatrix} E_x \\ E_y \\ -aE_x - bE_y \\ cE_x + aE_y \end{bmatrix}, \qquad \Psi_0^R = \begin{bmatrix} \rho_x \\ \rho_y \\ a\rho_x + b\rho_y \\ -c\rho_x - a\rho_y \end{bmatrix}, \qquad \Psi^T = \begin{bmatrix} \tau_x \\ \tau_y \\ -a\tau_x - b\tau_y \\ c\tau_x + a\tau_y \end{bmatrix} \qquad (B.1)$$

Where the coefficients, (a, b, c) are defined by Equation 1.10 and T is the 4 x 4 transfer matrix. To determine the transmission and reflection coefficients, we simply need to collect terms.

$$\begin{bmatrix} \tau_x \\ \tau_y \\ -a\tau_x - b\tau_y \\ c\tau_x + a\tau_y \end{bmatrix} = T \begin{bmatrix} E_x \\ E_y \\ -aE_x - bE_y \\ cE_x + aE_y \end{bmatrix} + T \begin{bmatrix} \rho_x \\ \rho_y \\ a\rho_x + b\rho_y \\ -c\rho_x - a\rho_y \end{bmatrix} \qquad (B.2)$$

Then

$$\begin{bmatrix} \tau_x \\ \tau_y \\ -a\tau_x - b\tau_y \\ c\tau_x + a\tau_y \end{bmatrix} - \begin{bmatrix} T_{11}\rho_x + T_{22}\rho_y + aT_{13}\rho_x + bT_{13}\rho_y - cT_{14}\rho_x - aT_{14}\rho_y \\ T_{21}\rho_x + T_{22}\rho_y + aT_{23}\rho_x + bT_{23}\rho_y - cT_{24}\rho_x - aT_{24}\rho_y \\ T_{31}\rho_x + T_{32}\rho_y + aT_{33}\rho_x + bT_{33}\rho_y - cT_{34}\rho_x - aT_{34}\rho_y \\ T_{41}\rho_x + T_{42}\rho_y + aT_{43}\rho_x + bT_{43}\rho_y - cT_{44}\rho_x - aT_{44}\rho_y \end{bmatrix} = \hat{T} \begin{bmatrix} E_x \\ E_y \\ -aE_x - bE_y \\ cE_x + aE_y \end{bmatrix}$$

$$\begin{bmatrix} 1 & 0 & -(T_{11} + aT_{13} - cT_{14}) & -(T_{12} + bT_{13} - aT_{14}) \\ 0 & 1 & -(T_{21} + aT_{23} - cT_{24}) & -(T_{22} + bT_{23} - aT_{24}) \\ -a & -b & -(T_{31} + aT_{33} - cT_{34}) & -(T_{32} + bT_{33} - aT_{34}) \\ c & a & -(T_{41} + aT_{43} - cT_{44}) & -(T_{42} + bT_{43} - aT_{44}) \end{bmatrix} \begin{bmatrix} \tau_x \\ \tau_y \\ \rho_x \\ \rho_y \end{bmatrix} = \hat{T} \begin{bmatrix} E_x \\ E_y \\ -aE_x - bE_y \\ cE_x + aE_y \end{bmatrix}$$

$$\hat{\Gamma} \begin{bmatrix} \tau_x \\ \tau_y \\ \rho_x \\ \rho_y \end{bmatrix} = \hat{T} \begin{bmatrix} E_x \\ E_y \\ -aE_x - bE_y \\ cE_x + aE_y \end{bmatrix}$$

$$\begin{bmatrix} \tau_x \\ \tau_y \\ \rho_x \\ \rho_y \end{bmatrix} = \hat{\Gamma}^{-1}\hat{T} \begin{bmatrix} E_x \\ E_y \\ -aE_x - bE_y \\ cE_x + aE_y \end{bmatrix}$$

$$(B.3)$$

One needs only the elements of the transfer matrix and the values of the coefficients (a, b, c) to determine $\hat{\Gamma}$ (and thus $\hat{\Gamma}^{-1}$). The values of (E_x, E_y) are the starting polarization of the wave. For example, if we only have $(1,0)$, then it is x polarized; if we have $(0,1)$, then it is y polarized.

APPENDIX C: DERIVATION OF THE MAGNETIC PERMEABILITY TENSOR

In section 4.2, we introduce the equation of motion of magnetization, (4.1), which is used to describe the motion of magnetization inside a ferromagnet when under the influence of both a steady magnetic field as well as an alternating magnetic field; the alternating part is representative of electromagnetic radiation. In Appendix C, we will show the steps that derive the magnetic permeability tensor, μ. For a more details, see Ref. [33].

We start with the equation of motion of magnetization (Equation 4.1), and consider a steady and oscillating (AC) magnetic field and magnetization (Equation 4.2). Substituting equation 4.2 into equation 4.1,

$$\frac{\partial \vec{M}_0}{\partial t} + \frac{\partial \vec{m}_\sim}{\partial t} = -\gamma\left(\vec{M}_0 \times \vec{H}_0 + \vec{M}_0 \times \vec{h}_\sim + \vec{m}_\sim \times \vec{H}_0 + \vec{m}_\sim \times \vec{h}_\sim\right) \tag{C.1}$$

We assume that the steady magnetic field, $\vec{H}_0$, and corresponding magnetization, $\vec{M}_0$, both point along the same direction (we will consider the $\hat{z}$ axis for this direction). Also we will assume the AC components to be much smaller than their steady counterparts:

$$\vec{H}_0 \times \vec{M}_0 = 0, \qquad \vec{h}_\sim \ll \vec{H}_0, \qquad \vec{m}_\sim \ll \vec{M}_0 \tag{C.2}$$

Additionally, we will assume that the magnitude of the steady magnetization to remain constant. This is assuming that the magnetization only rotates in response to the magnetic field, but doesn't change in length. This leads to Equation C.3 (or Equation 4.4).

$$\frac{\partial \vec{m}_\sim}{\partial t} + \gamma \vec{m}_\sim \times \vec{H}_0 = -\gamma \vec{M}_0 \times \vec{h}_\sim \tag{C.3}$$

Again, the angular momentum $\hat{J}$ is an operator that changes value in units of $\hbar$. This new equation now shows how a time changing Magnetization $\vec{M}$ relates to the normal of that same

Magnetization and the Magnetic Field $\vec{H}$. This equation does not allow for losses (losses will be included later). Two important assumptions will be made:

$$\vec{M} = \vec{M}_0 + \vec{m}_\sim, \qquad \vec{H} = \vec{H}_0 + \vec{h}_\sim \qquad (C.4)$$

Additionally, we will assume the length of $\vec{M}$ will not change ($\frac{\partial}{\partial t}M^2 = 0$). The vectors $\vec{m}_\sim$ and $\vec{h}_\sim$ are assumed to be much smaller than their respective $\vec{M}_0$ and $\vec{H}_0$ as to be tiny oscillations about a fixed vector, say the z direction:

$$\vec{M}_0 = M_0 \hat{z}, \qquad \vec{H}_0 = H_0 \hat{z}, \qquad \vec{M}_0 \times \vec{H}_0 = 0, \qquad \frac{\partial M_0}{\partial t} = \frac{\partial H_0}{\partial t} = 0 \qquad (C.5)$$

This alone reduces our lossless Magnetization equation of motion to:

$$\frac{\partial}{\partial t}\left(\vec{M}_0 + \vec{m}_\sim\right) = -\gamma\left(\vec{M}_0 + \vec{m}_\sim\right) \times \left(\vec{H}_0 + \vec{h}_\sim\right)$$

$$\left(\frac{\partial}{\partial t}\vec{M}_0 + \frac{\partial}{\partial t}\vec{m}_\sim\right) = -\gamma\left(\vec{M}_0 \times \vec{H}_0 + \vec{M}_0 \times \vec{h}_\sim + \vec{m}_\sim \times \vec{H}_0 + \vec{m}_\sim \times \vec{h}_\sim\right)$$

$$\frac{\partial}{\partial t}\vec{m}_\sim + \gamma \vec{m}_\sim \times \vec{H}_0 = -\gamma \vec{M}_0 \times \vec{h}_\sim \qquad (C.6)$$

Since we are considering tiny oscillations for the vectors $\vec{m}_\sim$ and $\vec{h}_\sim$:

$$\vec{m}_\sim = \vec{m}e^{i\omega t}, \qquad \vec{h}_\sim = \vec{h}e^{i\omega t} \qquad (C.7)$$

The convention here is for negative complex i (as usually the time component is $-i\omega t$ in the exponent. We will keep track of this. With this implemented, we obtain

$$i\omega\vec{m} + \gamma\vec{m} \times \vec{H}_0 = -\gamma\vec{M}_0 \times \vec{h} \qquad (C.8)$$

We can determine the Cartesian components by expanding the cross product.

$$i\omega m_x + \gamma m_y H_0 = \gamma M_0 h_y$$

$$-\gamma m_x H_0 + i\omega m_y = -\gamma M_0 h_x$$

$$i\omega m_z = 0 \qquad\qquad (C.9)$$

This set of linear equations can be written in a linear matrix format $\vec{m} = \chi \vec{h}$ where

$$\overleftrightarrow{\chi} = \begin{vmatrix} \chi & i\chi_a & 0 \\ -i\chi_a & \chi & 0 \\ 0 & 0 & 0 \end{vmatrix} \qquad\qquad (C.10)$$

$$\chi = \frac{\gamma M_0 \omega_H}{\omega_H^2 - \omega^2}, \qquad \chi_a = \frac{\gamma M_0 \omega}{\omega_H^2 - \omega^2}, \qquad \omega_H = \gamma H_0 \qquad\qquad (C.11)$$

Where equation C.10 is the same as 4.6 and equations C.11 are the same as 4.7 and 4.8. If we start with the system of equations (G&M eq. 1.37):

$$i\omega m_x + \gamma m_y H_0 = \gamma M_0 h_y$$

$$-\gamma m_x H_0 + i\omega m_y = -\gamma M_0 h_x$$

$$i\omega m_z = 0$$

We can write this in matrix form:

$$\begin{vmatrix} i\omega & \omega_H & 0 \\ -\omega_H & i\omega & 0 \\ 0 & 0 & i\omega \end{vmatrix} \begin{vmatrix} m_x \\ m_y \\ m_z \end{vmatrix} = \begin{vmatrix} 0 & \gamma M_0 & 0 \\ -\gamma M_0 & 0 & 0 \\ 0 & 0 & 0 \end{vmatrix} \begin{vmatrix} h_x \\ h_y \\ h_z \end{vmatrix}$$

Where we have already implemented the $\omega_H = \gamma H_0$. Now let us take the inverse of the coefficient matrix to the magnetization column matrix; recalling that $A^{-1} = \frac{1}{|A|}(C^T)_{ij}$, that is where

$$A = \begin{vmatrix} i\omega & \omega_H & 0 \\ -\omega_H & i\omega & 0 \\ 0 & 0 & i\omega \end{vmatrix}, \qquad A^T = \begin{vmatrix} i\omega & -\omega_H & 0 \\ \omega_H & i\omega & 0 \\ 0 & 0 & i\omega \end{vmatrix}, \qquad |A| = i\omega(\omega_H^2 - \omega^2)$$

Then

$$|A|^{-1} = \frac{1}{i\omega(\omega_H^2 - \omega^2)} \begin{vmatrix} [(i\omega)^2 - 0] & -[(i\omega\omega_H) - 0] & 0 \\ -[(-i\omega\omega_H) - 0] & [(i\omega)^2 - 0] & 0 \\ 0 & 0 & (\omega_H^2 - \omega^2) \end{vmatrix}$$

Then

$$\begin{vmatrix} m_x \\ m_y \\ m_z \end{vmatrix} = \frac{1}{i\omega(\omega_H^2 - \omega^2)} \begin{vmatrix} -\omega^2 & -i\omega\omega_H & 0 \\ i\omega\omega_H & -\omega^2 & 0 \\ 0 & 0 & (\omega_H^2 - \omega^2) \end{vmatrix} \begin{vmatrix} 0 & \gamma M_0 & 0 \\ -\gamma M_0 & 0 & 0 \\ 0 & 0 & 0 \end{vmatrix} \begin{vmatrix} h_x \\ h_y \\ h_z \end{vmatrix}$$

$$\begin{vmatrix} m_x \\ m_y \\ m_z \end{vmatrix} = \frac{1}{i\omega(\omega_H^2 - \omega^2)} \begin{vmatrix} \gamma M_0 \omega \omega_H i & -\gamma M_0 \omega^2 & 0 \\ \gamma M_0 \omega^2 & \gamma M_0 \omega \omega_H i & 0 \\ 0 & 0 & 0 \end{vmatrix} \begin{vmatrix} h_x \\ h_y \\ h_z \end{vmatrix}$$

$$\begin{vmatrix} m_x \\ m_y \\ m_z \end{vmatrix} = \begin{vmatrix} \dfrac{\gamma M_0 \omega_H}{\omega_H^2 - \omega^2} & \dfrac{\gamma M_0 \omega}{\omega_H^2 - \omega^2} i & 0 \\ -\dfrac{\gamma M_0 \omega}{\omega_H^2 - \omega^2} i & \dfrac{\gamma M_0 \omega_H}{\omega_H^2 - \omega^2} & 0 \\ 0 & 0 & 0 \end{vmatrix} \begin{vmatrix} h_x \\ h_y \\ h_z \end{vmatrix}$$

Hence

$$\overleftrightarrow{\chi} = \begin{vmatrix} \chi & \chi_a i & 0 \\ -\chi_a i & \chi & 0 \\ 0 & 0 & 0 \end{vmatrix}$$

Where

$$\chi = \frac{\gamma M_0 \omega_H}{\omega_H^2 - \omega^2}, \qquad \chi_a = \frac{\gamma M_0 \omega}{\omega_H^2 - \omega^2}, \qquad \omega_H = \gamma H_0$$

Which satisfies eq. 1.42 in G&M.

Finding the permeability Tensor

$$\mu = 1 + 4\pi\chi$$

$$\mu = 1 + 4\pi \frac{\gamma M_0 \omega_H}{\omega_H^2 - \omega^2}$$

$$\mu = \frac{\omega_H^2 - \omega^2}{\omega_H^2 - \omega^2} + \frac{\omega_M \omega_H}{\omega_H^2 - \omega^2}$$

$$\mu = \frac{\omega_H^2 - \omega^2 + \omega_M \omega_H}{\omega_H^2 - \omega^2}$$

$$\mu = \frac{\omega_H(\omega_H + \omega_M) - \omega^2}{\omega_H^2 - \omega^2}$$

VITA

Kyle James Smith is from Austin, TX. He obtained his bachelors of Science in Physics at Texas State University in San Marcos, TX. and received his Ph.D. in Physics at the University of Texas at San Antonio. He's future plans include education in physics at the university level where students Kyle hopes to inspire students in physics the same way he was by his mentors

BIBLIOGRAPHY

1. Figotin, A. and I. Vitebskiy, *Absorption suppression in photonic crystals.* Physical Review B, 2008. **77**(10): p. 104421.
2. Yablonovitch, E., *Inhibited spontaneous emission in solid-state physics and electronics.* Physical Review Letters, 1987. **58**(20): p. 2059-2062.
3. John, S., *Strong localization of photons in certain disordered dielectric superlattices.* Physical Review Letters, 1987. **58**(23): p. 2486-2489.
4. Rayleigh, L., *XVII. On the maintenance of vibrations by forces of double frequency, and on the propagation of waves through a medium endowed with a periodic structure.* The London, Edinburgh, and Dublin Philosophical Magazine and Journal of Science, 1887. **24**(147): p. 145-159.
5. Macleod, H.A., *Thin-film optical filters.* 2001: CRC press.
6. Penselin, S. and A. Steudel, *Fabry-Perot-Interferometerverspiegelungen aus dielektrischen Vielfachschichten.* Zeitschrift für Physik, 1955. **142**(1): p. 21-41.
7. Yeh, P., *Optical waves in layered media.* Vol. 95. 1988: Wiley Online Library.
8. Kronig, R.d.L. and W. Penney. *Quantum mechanics of electrons in crystal lattices.* in *Proceedings of the Royal Society of London A: Mathematical, Physical and Engineering Sciences.* 1931. The Royal Society.
9. Vaughan, M., *The Fabry-Perot interferometer: history, theory, practice and applications.* 1989: CRC press.
10. Fabry, C. and A. Perot, *Theorie et applications d'une nouvelle methode de spectroscopie interferentielle.* Ann. Chim. Phys, 1899. **16**(7): p. 115.
11. Berning, P.H. and A. Turner, *Induced transmission in absorbing films applied to band pass filter design.* JoSA, 1957. **47**(3): p. 230-239.
12. Polster, H.D., *A symmetrical all-dielectric interference filter.* JOSA, 1952. **42**(1): p. 21-23.
13. Orfanidis, S.J., *Electromagnetic waves and antennas.* 2002: Rutgers University New Brunswick, NJ.
14. Sánchez-Soto, L.L., et al., *The transfer matrix: A geometrical perspective.* Physics Reports, 2012. **513**(4): p. 191-227.
15. Figotin, A. and I. Vitebskiy, *Oblique frozen modes in periodic layered media.* Physical Review E, 2003. **68**(3): p. 036609.
16. Berreman, D.W., *Optics in stratified and anisotropic media: 4×4-matrix formulation.* JoSA, 1972. **62**(4): p. 502-510.
17. Abdulhalim, I., *Analytic propagation matrix method for linear optics of arbitrary biaxial layered media.* Journal of Optics A: Pure and Applied Optics, 1999. **1**(5): p. 646.
18. Abdulhalim, I., *Reflective phase-only modulation using one-dimensional photonic crystals.* Journal of Optics A: Pure and Applied Optics, 2000. **2**(2): p. L9.
19. Holloway, R. and P. Lissberger, *The Design and Preparation of Induced Transmission Filters.* Applied optics, 1969. **8**(3): p. 653-660.
20. Landau, B. and P. Lissberger, *Theory of induced-transmission filters in terms of the concept of equivalent layers.* JoSA, 1972. **62**(11): p. 1258-1264.
21. Lide, D.R., *Handbook of Chemistry and Physics, The Chemical Rubber Company.* 1997, CRC Press, Boca Raton, Florida, USA.

22.   Smith, K. and A. Chabanov, *Enhanced Transmission and Nonreciprocal Properties of a Ferromagnetic Metal Layer in One-Dimensional Photonic Crystals.* Integrated Ferroelectrics, 2011. **131**(1): p. 66-71.

23.   Ralston, J. and R. Chang, *Optical limiting in semiconductors.* Applied Physics Letters, 1969. **15**(6): p. 164-166.

24.   Boggess, T., et al., *Optical limiting in GaAs.* IEEE journal of quantum electronics, 1985. **21**(5): p. 488-494.

25.   Boggess, T.F., et al., *Nonlinear-optical energy regulation by nonlinear refraction and absorption in silicon.* Optics letters, 1984. **9**(7): p. 291-293.

26.   Zvezdin, A.K. and V.A. Kotov, *Modern magnetooptics and magnetooptical materials.* 1997: Taylor & Francis.

27.   Pozar, D.M., *Microwave engineering.* 2009: John Wiley & Sons.

28.   Morrish, A.H., *The physical principles of magnetism.* The Physical Principles of Magnetism, by Allan H. Morrish, pp. 696. ISBN 0-7803-6029-X. Wiley-VCH, January 2001., 2001. **1**.

29.   Tamm, I.E., *Fundamentals of the Theory of Electricity.* 1949, Moscow: Gostekhizdat.

30.   Chikazumi, S., *Physics of Magnetism.* 1986, Malabar, Fl: Krieger Pub Co.

31.   Kittel, C., *Introduction to Solid State Physics.* 1976, New York: Wiley.

32.   Van Vleck, J., *Ferromagnetic Resonance.* Physica 1951. **17**(3/4): p. 234.

33.   Gurevich, A.G. and G.A. Melkov, *Magnetization oscillations and waves.* 1996: CRC.

34.   Polder, D., *VIII. On the theory of ferromagnetic resonance.* Philosophical magazine, 1949. **40**(300): p. 99-115.

35.   Landau, L.D. and E.M. Lifshitz, *Course of theoretical physics.* 2013: Elsevier.

36.   Arkadyev, V., K, *Absorption of Electric Waves in Parallel Wires.* Zh Russk. Fiz.-Khim Obshchestva, Otdel Fiz., 1912. **44**(4): p. 165.

37.   Dorfmann, J., *Some Comments to Understanding the Mechanism of Magnetic Phenomena.* Z. Phys.,, 1923. **17**(2): p. 98.

38.   Landau, L.D.L., E. M., *To the theory of the dispersion of the ferromagnetic-body permeability.* Collected Papers, ter Haar, D., Ed., Pergamon, Oxford, 1965.

39.   Griffiths, J., *Anomalous high-frequency resistance of ferromagnetic metals.* Nature, 1946. **158**(4019): p. 670.

40.   Skrotskiĭ, G., *The Landau-Lifshitz equation revisited.* Physics-Uspekhi, 1984. **27**(12): p. 977-979.

41.   Kittel, C., *On the theory of ferromagnetic resonance absorption.* Physical Review, 1948. **73**(2): p. 155.

42.   Landau, L. and E. Lifshitz, *On the theory of the dispersion of magnetic permeability in ferromagnetic bodies.* Phys. Z. Sowjetunion, 1935. **8**(153): p. 101-114.

43.   Aplet, L. and J. Carson, *A Faraday effect optical isolator.* Applied Optics, 1964. **3**(4): p. 544-545.

44.   Lyubchanskii, I., et al., *Magnetic photonic crystals.* Journal of Physics D: Applied Physics, 2003. **36**(18): p. R277.

45.   Levy, M., *The on-chip integration of magnetooptic waveguide isolators.* Selected Topics in Quantum Electronics, IEEE Journal of, 2002. **8**(6): p. 1300-1306.

46.   Inoue, M., et al., *Magnetophotonic crystals.* Journal of Physics D: Applied Physics, 2006. **39**(8): p. R151.

47. Sakaguchi, S. and N. Sugimoto, *Transmission properties of multilayer films composed of magneto-optical and dielectric materials*. Lightwave Technology, Journal of, 1999. **17**(6): p. 1087-1092.

48. Inoue, M., et al., *Magneto-optical properties of one-dimensional photonic crystals composed of magnetic and dielectric layers*. Journal of applied physics, 1998. **83**(11): p. 6768-6770.

49. Hamon, T., et al., *Investigation of a one-dimensional magnetophotonic crystal for the study of ultrathin magnetic layer*. Journal of Physics D: Applied Physics, 2006. **39**(6): p. 1012.

50. Inoue, M., et al., *One-dimensional magnetophotonic crystals*. Journal of applied physics, 1999. **85**(8): p. 5768-5770.

51. Shimizu, H., M. Miyamura, and M. Tanaka, *Enhanced magneto-optical effect in a GaAs: MnAs nanoscale hybrid structure combined with GaAs/AlAs distributed Bragg reflectors*. Journal of Vacuum Science & Technology B: Microelectronics and Nanometer Structures, 2000. **18**(4): p. 2063-2065.

52. Kahl, S. and A.M. Grishin, *Enhanced Faraday rotation in all-garnet magneto-optical photonic crystal*. Applied physics letters, 2004. **84**(9): p. 1438-1440.

53. Shuvaev, A., et al., *Giant magneto-optical Faraday effect in HgTe thin films in the terahertz spectral range*. Physical Review Letters, 2011. **106**(10): p. 107404.

54. Goto, T., et al., *Optical Tamm states in one-dimensional magnetophotonic structures*. Physical Review Letters, 2008. **101**(11): p. 113902.

55. Steel, M., M. Levy, and R. Osgood Jr, *High transmission enhanced Faraday rotation in one-dimensional photonic crystals with defects*. Photonics Technology Letters, IEEE, 2000. **12**(9): p. 1171-1173.

56. Steel, M., M. Levy, and R. Osgood, *Photonic bandgaps with defects and the enhancement of Faraday rotation*. Journal of lightwave technology, 2000. **18**(9): p. 1297.

57. Kato, H., et al., *Effect of optical losses on optical and magneto-optical properties of one-dimensional magnetophotonic crystals for use in optical isolator devices*. Optics communications, 2003. **219**(1): p. 271-276.

58. Atkinson, R., *Limits of enhancement of the Faraday effect in ultra-thin magnetic layers by one-dimensional magnetophotonic crystals*. Journal of Physics D: Applied Physics, 2006. **39**(6): p. 999.

59. Kaplan, A., *On the reflectivity of metallic films at microwave and radio frequencies(Radio wave reflection on thin metallic films in superhigh frequency and radio range as function of thickness and temperature)*. RADIO ENGINEERING AND ELECTRONIC PHYSICS, 1964. **9**: p. 1476-1481.

60. Frait, Z. and H. MacFaden, *Ferromagnetic Resonance In Metals Frequency Dependence*. Physical Review, 1965. **139**(4): p. 1173-1181.

61. Hogan, C., *The ferromagnetic Faraday effect at microwave frequencies and its applications*. Reviews of Modern Physics, 1953. **25**(1): p. 253.

62. Palik, E. and J. Furdyna, *Infrared and microwave magnetoplasma effects in semiconductors*. Reports on Progress in Physics, 2002. **33**(3): p. 1193.

63. Yariv, A., et al., *Coupled-resonator optical waveguide: a proposal and analysis*. Optics Letters, 1999. **24**(11): p. 711-713.

64. Ye, Y.H., et al., *Finite-size effect on one-dimensional coupled-resonator optical waveguides*. Physical Review E, 2004. **69**(5): p. 056604.

65.	Ghulinyan, M., et al., *Wide-band transmission of nondistorted slow waves in one-dimensional optical superlattices.* Applied physics letters, 2006. **88**(24): p. 241103-241103-3.